

Salt-responsive gut commensal modulates TH17 axis and disease

Peer-reviewed author version

Wilck, Nicola; Matus, Mariana G.; Kearney, Sean M.; Olesen, Scott W.; Forslund, Kristoffer; Bartolomeus, Hendrik; Jörg, Stefanie; Mähler, Anja; Balogh, András; Markó, Lajos; Vvedenskaya, Olga; Kleiner, Friedrich H.; Tsvetkov, Dmitry; Klug, Lars; Costea, Paul I.; Sunagawa, Shinichi; Maier, Lisa; Rakova, Natalia; Schatz, Valentin; Neubert, Patrick; Frätzer, Christian; Krannich, Alexander; Gollasch, Maik; Grohme, Diana A.; Côte-Real, Beatriz F.; Gerlach, Roman G.; Basic, Marijana; Typas, Athanasios; Wu, Chuan; Titze, Jens M.; Jantsch, Jonathan; Boschmann, Michael; Dechend, Ralf; KLEINewIETFELD, Markus; Kempa, Stefan; Bork, Peer; Linker, Ralf A.; Alm, Eric J. & Müller, Dominik N. (2017) Salt-responsive gut commensal modulates TH17 axis and disease. In: NATURE, 551(7682), p. 585-589.

DOI: 10.1038/nature24628

Handle: <http://hdl.handle.net/1942/25993>

1 **Salt-responsive gut commensal modulates T_H17 axis and disease**

2

3 **Short title:** Salt and gut microbiome

4

5 Nicola Wilck^{1,2,3,4,5}, Mariana G. Matus^{6,7}, Sean M. Kearney⁶, Scott W. Olesen⁶, Kristoffer
6 Forslund⁸, Hendrik Bartolomeaus^{1,2,3,4}, Stefanie Jörg⁹, Anja Mähler^{1,5}, András Balogh^{1,2,3,4,5},
7 Lajos Markó^{1,2,3,4,5}, Olga Vvedenskaya^{3,10,11}, Friedrich H. Kleiner¹, Dmitry Tsvetkov^{1,2}, Lars
8 Klug^{1,5}, Paul I. Costea⁸, Shinichi Sunagawa^{8,12}, Lisa Maier¹³, Natalia Rakova^{1,9}, Valentin
9 Schatz¹⁴, Patrick Neubert¹⁴, Christian Frätzer¹⁵, Alexander Krannich⁵, Maik Gollasch^{1,2,3}, Diana
10 A. Grohme¹⁶, Beatriz F. Côrte-Real²², Roman G. Gerlach¹⁷, Marijana Basic¹⁸, Athanasios
11 Typas¹³, Chuan Wu¹⁹, Jens M. Titze²⁰, Jonathan Jantsch¹⁴, Michael Boschmann^{1,5}, Ralf
12 Dechend^{1,2,5}, Markus Kleinewietfeld^{16,21,22}, Stefan Kempa^{3,5,10}, Peer Bork^{3,8,23,24}, Ralf A.
13 Linker^{9*}, Eric J. Alm^{6*}, Dominik N. Müller^{1,2,3,4,5*}

14

15 **Affiliations**

16 ¹Experimental and Clinical Research Center, a joint cooperation of Max-Delbrück Center for
17 Molecular Medicine and Charité-Universitätsmedizin Berlin, 13125 Berlin, Germany

18 ²Charité-Universitätsmedizin Berlin, 10117 Berlin, Germany

19 ³Max-Delbrück Center for Molecular Medicine in the Helmholtz Association, 13125 Berlin,
20 Germany

21 ⁴DZHK (German Centre for Cardiovascular Research), partner site Berlin, Germany

22 ⁵Berlin Institute of Health (BIH), Berlin, Germany

23 ⁶Center for Microbiome Informatics and Therapeutics, and Department of Biological
24 Engineering, Massachusetts Institute of Technology, Cambridge, Massachusetts 02139, USA

25 ⁷Computational and Systems Biology Program, Massachusetts Institute of Technology,
26 Cambridge, Massachusetts 02139, USA

27 ⁸European Molecular Biology Laboratory, Structural and Computational Biology Unit, 69117
28 Heidelberg, Germany

29 ⁹Department of Neurology, Friedrich-Alexander-University Erlangen-Nuremberg, 91054
30 Erlangen, Germany

31 ¹⁰Integrative Proteomics and Metabolomics Platform, Berlin Institute for Medical Systems
32 Biology BIMS, 13125 Berlin, Germany

33 ¹¹Berlin School of Integrative Oncology, Charité University Medicine Berlin, Germany

34 ¹²Institute of Microbiology, ETH Zurich, 8092 Zurich, Switzerland

35 ¹³European Molecular Biology Laboratory, Genome Biology Unit, 69117 Heidelberg,
36 Germany

37 ¹⁴Institute of Clinical Microbiology and Hygiene, University Hospital of Regensburg,
38 University of Regensburg, 93053 Regensburg, Germany

39 ¹⁵Lipidomix GmbH, 13125 Berlin, Germany

40 ¹⁶Translational Immunology, Department of Clinical Pathobiochemistry, Medical Faculty
41 Carl Gustav Carus, TU Dresden, 01307 Dresden, Germany

42 ¹⁷Project Group 5, Robert Koch Institute, 38855 Wernigerode, Germany

43 ¹⁸Hannover Medical School, Institute for Laboratory Animal Science and Central Animal
44 Facility, 30625 Hannover, Germany

45 ¹⁹Experimental Immunology Branch, National Cancer Institute, US National Institutes of
46 Health, Bethesda, Maryland, USA

47 ²⁰Division of Clinical Pharmacology, Vanderbilt University School of Medicine, Nashville,
48 Tennessee, USA

49 ²¹Center for Regenerative Therapies Dresden (CRTD), 01307 Dresden, Germany

50 ²²VIB Laboratory of Translational Immunomodulation, VIB Center for Inflammation
51 Research (IRC), UHasselt, Campus Diepenbeek, 3590 Diepenbeek, Belgium

52 ²³Molecular Medicine Partnership Unit, University of Heidelberg and European Molecular

53 Biology Laboratory, 69120 Heidelberg, Germany

54 ²⁴Department of Bioinformatics, Biocenter, University of Würzburg, 97074 Würzburg,

55 Germany

56 * These authors contributed equally to this work.

57

58 **Corresponding authors:** D.N.M. dominik.mueller@mdc-berlin.de, E.J.A. ejalm@mit.edu

59 Western lifestyle with high salt consumption leads to hypertension and cardiovascular disease.
60 High salt may additionally drive autoimmunity by inducing T helper (T_H)17 cells, which may
61 also contribute to hypertension. Induction of T_H17 cells depends on the gut microbiota, yet the
62 effect of salt on the gut microbiome is unknown. In mouse model systems, we show that high
63 salt intake affects the gut microbiome, particularly by depleting *Lactobacillus murinus*.
64 Consequently, *L. murinus* treatment prevents salt-induced aggravation of actively-induced
65 experimental autoimmune encephalomyelitis and salt-sensitive hypertension, by modulating
66 T_H17 cells. In line with these findings, moderate high salt challenge in a pilot study in humans
67 reduces intestinal survival of *Lactobacillus spp.* along with increased T_H17 cells and blood
68 pressure. Our results connect high salt intake to the gut-immune axis and highlight the gut
69 microbiome as a potential therapeutic target to counteract salt-sensitive conditions.

70 High salt content in the Western diet is implicated in numerous disorders¹, particularly
71 cardiovascular disease². Guidelines^{3,4} and public initiatives recommend reducing salt intake,
72 yet an improved mechanistic understanding is warranted. The deleterious effect of a high salt
73 diet (HSD) on cardiovascular health is driven by arterial hypertension and associated with
74 increased morbidity and mortality^{2,5}. Thus far, most studies have focused on the role of the
75 kidneys, the sympathetic nervous system, and direct effects on the vasculature⁶. However, some
76 investigations implicate the immune system in these processes⁷ linking pro-inflammatory T
77 cells to the development of hypertension⁸. In particular, interleukin (IL)-17A producing CD4⁺
78 helper T cells (T_H17) may promote hypertension^{9,10}. T_H17 cells play a deleterious role in
79 autoimmune diseases. We and others recently demonstrated that the generation of pathogenic
80 T_H17 cells could be promoted by a high salt environment. Consequently, a HSD boosts T_H17
81 generation and exacerbates actively-induced experimental autoimmune encephalomyelitis
82 (EAE)^{11,12}, as a prototypic T_H17-driven autoimmune disease¹³. Active MOG₃₅₋₅₅-induced EAE
83 is a disease model recapitulating many aspects of multiple sclerosis (MS), although differing
84 from transgenic EAE models in several aspects of T cell function¹⁴. The intestine is exposed
85 to varying salt loads of ingested foods, yet the interaction between HSD and the gut microbiome
86 has not been thoroughly investigated. Gut microbes are known to respond to fluctuations in
87 dietary composition¹⁵, leading to transient or persistent alterations of the gut microbiome¹⁶.
88 Diet-induced shifts in microbiome composition may have profound effects on the host,
89 especially on T cells¹⁷. T_H17 cells are particularly affected by the abundance of specific
90 commensal bacteria¹⁸. We sought to examine the influence of high salt challenges on the gut
91 microbiome, the immune system, and implications for hypertension and autoimmunity.

92

93 **High salt decreases *Lactobacillus* in mice**

94 To determine the effect of a HSD on the gut microbiome composition, we analyzed fecal
95 pellets from normal salt diet (NSD) or HSD-fed FVB/N mice by 16S ribosomal DNA (rDNA)
96 gene sequencing. Both diets were equally well-tolerated, indicated by similar body weight and
97 food intake (Extended Data Fig. 1a, b). HSD-fed mice had a significantly higher fluid and salt
98 intake than NSD-fed mice (Extended Data Fig. 1c-f), but similar intestinal transit (Extended
99 Data Fig. 1g). The overall microbial composition (based on Operational Taxonomic Units,
100 OTUs, assigned using Ribosomal Database Project, RDP) showed no obvious pattern shifts
101 between HSD and NSD mice (Extended Data Fig. 2a, b, 3a). Although Jensen-Shannon
102 Divergence indicated differences between HSD and NSD bacterial communities, these
103 differences were not confirmed by Bray-Curtis or UniFrac metrics (data not shown). Bacterial
104 load was not significantly different between NSD and HSD (Extended Data Fig. 3b), but several
105 OTUs were significantly decreased under HSD on day 14, including species with the genera
106 *Lactobacillus*, *Oscillibacter*, *Pseudoflavonifractor*, *Clostridium XIVa*, *Johnsonella* and *Rothia*,
107 while others increased under HSD, e.g. *Parasutterella spp.* (Extended Data Fig. 3c).
108 Interestingly, analysis of fecal metabolites from central carbon and nitrogen metabolic
109 pathways by gas-chromatography mass-spectrometry showed clear differences between the two
110 groups (Extended Data Fig. 3d-g). The absence of large-scale taxonomic differences was
111 unexpected, given the differences in metabolites, but consistent with the fact that the two diets
112 are identical in energy content and only differ in salt content. To identify the specific bacterial
113 OTUs that did change across diet, we employed a sensitive machine learning approach. An
114 AdaBoost classifier trained to distinguish NSD from HSD samples on day 14 of the treatment
115 identified 8 OTUs with nontrivial feature importance (Figure 1a, c) with 92% accuracy (Figure
116 1b). These OTUs varied in maximum relative abundance (from 0.04% to 19.5%) and responded
117 differently to the HSD (Figure 1a, c). OTUs identified as most important were consistent across
118 different cross-validation runs, and across different algorithms (Extended Data Fig. 4a). The

119 most important OTU (25% feature importance) was a member of the genus *Lactobacillus*, and
120 was depleted under HSD (Figure 1d). Other features included OTUs from *Prevotellaceae*,
121 *Pseudoflavonifractor*, *Clostridia*, *Parasutterella*, *Akkermansia*, *Bacteroidetes* and *Alistipes*
122 (Figure 1a, c, Extended Data Fig. 4b). *Lactobacillus* depletion showed a quick onset detectable
123 1 day after initiation of the HSD, remaining at low levels during the HSD with the lowest
124 abundance on day 14. When the mice were returned to NSD, the *Lactobacillus* OTU abundance
125 returned to baseline levels (Figure 1d).

126 Since the *Lactobacillus* OTU was the bacterial group most strongly associated with high salt,
127 we aimed to isolate a *Lactobacillus* strain from the mouse feces. The 16S rDNA sequence of
128 the isolate shared 100% identity with the V4-V5 16S region of the OTU described above, and
129 was identified as *L. murinus*. We confirmed the decrease of this strain under HSD using qPCR
130 (Figure 1e, f). Genome sequencing of the isolate showed 93% similarity to two published *L.*
131 *murinus* genomes^{19,20} (Extended Data Fig. 5a). Notably, there are no strains of *L. murinus*
132 known to be native to the human microbiota, with the closest 16S sequence in the human gut
133 microbiota matching at below 90% identity (Extended Data Fig. 5b). The prevalence of
134 different *Lactobacillus* species varies in humans, each present in 0.5-22% of subjects in the
135 MetaHIT²¹ Danish subcohort (Extended Data Fig. 5b).

136 Next, we cultured *L. murinus*, human-associated *Lactobacilli* and non-related control strains
137 *in vitro* and tested their growth under increasing NaCl concentrations. Half maximal growth
138 inhibition (IC₅₀) of *L. murinus* occurred at comparable NaCl concentrations under aerobic and
139 anaerobic culture conditions (Extended Data Fig. 5c, d). NaCl inhibited the growth of several
140 human isolates at slightly lower concentrations, with the exception of *L. salivarius* (Extended
141 Data Fig. 5e, f). However, not all strains tested were similarly salt-sensitive. For instance,
142 *Akkermansia muciniphila*, identified by the classifier and increasing in fecal abundance upon
143 HSD, and *Escherichia coli* had higher salt tolerances (Extended Data Fig. 5d, g). Importantly,

144 *in vivo* colonic fecal sodium concentrations in HSD-fed mice are comparable to growth
145 inhibitory NaCl concentrations *in vitro* (0.252 for HSD vs. 0.133 M for NSD).

146 Since *Lactobacilli* are known to metabolize tryptophan to indole metabolites²², we
147 speculated that HSD would also reduce fecal indoles. Indeed, HSD significantly reduced fecal
148 levels of indole-3-lactic acid (ILA, Figure 1g) and indole-3-acetic acid (IAA, Extended Data
149 Fig. 6a), while indole-3-carboxaldehyde was unchanged (IAld, Extended Data Fig. 6b).
150 Notably, mice monocolonized with the *L. murinus* isolate exhibited fecal ILA, IAA and IAld
151 as compared to germ-free (GF) controls, indicating *L. murinus* capability of producing these
152 indoles (Figure 1h, Extended Data Fig. 6c-d).

153

154 ***L. murinus* ameliorates active EAE**

155 In MS²³ and EAE²⁴, the importance of the gut microbiome has recently been recognized.
156 The suppression of *L. murinus* by HSD prompted us to investigate whether oral administration
157 of *L. murinus* ameliorates HSD-induced exacerbation of actively-induced MOG₃₅₋₅₅ EAE.
158 We relied on a daily gavage protocol to maintain *L. murinus* abundance and fecal indole
159 metabolites during HSD. Body weight and disease incidence were similar in all groups. Mice
160 on a HSD displayed an exacerbated disease course (Figure 2a; Extended Data Fig. 7a). *L.*
161 *murinus* supplementation during HSD and NSD feeding ameliorated the disease (Figure 2a and
162 Extended Data Fig. 7a, b). Similar results were observed when HSD-fed mice were treated with
163 *L. reuteri* (Extended Data Fig. 7c). We analyzed small intestinal *lamina propria* (siLPL) CD4⁺
164 lymphocytes producing IL-17A by flow cytometry at the maximum of intestinal T_H17
165 expansion on day 3 post MOG immunization (p.i.)²⁵. HSD mice displayed a significantly higher
166 frequency of T_H17 cells compared to NSD mice, which was reduced in HSD-fed mice
167 concomitantly receiving *L. murinus* (Figure 2b). Flow cytometry analysis of splenocytes and
168 spinal cord infiltrating lymphocytes on day 17 p.i. revealed a significant reduction in T_H17 cells
169 by *L. murinus* (Figure 2c, d) and by *L. reuteri* treatment (Extended Data Fig. 7d, e) compared

170 to HSD feeding alone. mRNA expression of *Il17a* and *Rorc* in spinal cord tissue was decreased
171 after *L. murinus* treatment with a tendency towards lower *Csf2* levels (Extended Data Figure
172 7f-h). The effect of HSD and *L. murinus* was largely T_H17 specific as interferon (IFN)- γ
173 producing CD4⁺ lymphocytes were not affected in siLPL, spleen or spinal cord (Extended Data
174 Fig. 7i). Since we focused on actively-induced MOG₃₅₋₅₅-EAE further studies are needed to
175 extend the concept for HSD and *Lactobacillus* treatment to spontaneous EAE.

176 To elaborate on putative mechanisms for the modulation of T_H17 cells, we focused on fecal
177 indole metabolites, which are known to improve actively-induced EAE²⁶. HSD significantly
178 reduced fecal ILA, while concomitant *L. murinus* supplementation prevented this effect (Figure
179 3a, b). A similar pattern was observed for fecal IAA and IAld (Extended Data Fig. 7j-m). Next,
180 we investigated the effect of ILA on the differentiation of murine T_H17 cells *in vitro*. ILA
181 significantly reduced T_H17 polarization in a dose-dependent manner (Figure 3c).

182 However, in MOG₃₅₋₅₅ immunized GF mice, HSD did not change T_H17 frequencies
183 compared to NSD (Extended Data Fig. 8a, b), indicating a crucial role for intestinal bacteria in
184 mediating the HSD effect on T_H17 cells. To corroborate the modulatory effects of *L. murinus*,
185 we used segmented filamentous bacteria (SFB) as known inducers of intestinal T_H17 cells¹⁸ and
186 compared MOG₃₅₋₅₅ immunization in gnotobiotic mice harboring either solely SFB (GF+SFB)
187 or SFB and *L. murinus* (GF+SFB+*L. murinus*). As predicted, the presence or absence of *L.*
188 *murinus* determined T_H17 frequencies in siLPL and cLPL (Extended Data Fig. 8c, d).

189

190 ***L. murinus* reduces salt-sensitive hypertension**

191 Accumulating evidence suggests that T_H17 cells play a role in the genesis of hypertension⁷.
192 Moreover, a recent meta-analysis provided preliminary support that *Lactobacillus*-rich
193 probiotics might affect blood pressure in hypertensive subjects²⁷. Thus, we tested whether *L.*
194 *murinus* treatment would decrease experimental salt-sensitive hypertension.

195 Blood pressure increased over 3 weeks of HSD (Figure 4a, b, Extended Data Figure 9a).
196 Concomitant daily treatment with *L. murinus* led to a significant reduction of systolic and
197 normalization of diastolic blood pressure (Figure 4a, b, Extended Data Fig. 9b, c). *L. reuteri*
198 was similarly effective, while non-*Lactobacillus* strain *E. coli* Nissle 1917 was ineffective
199 (Extended Data Fig. 9d-g).

200 We next asked if *L. murinus* treatment affects T_H17 cells in experimental salt-sensitive
201 hypertension and analyzed intestinal and splenic lymphocytes by flow cytometry. Compared to
202 NSD, HSD led to a significant increase in CD4⁺RORγt⁺ T_H17 cell frequencies in siLPL, which
203 was significantly reduced by *L. murinus* treatment (Figure 4c). In addition, flow cytometry
204 analysis of siLPL, cLPL and splenic lymphocytes revealed a significant reduction of T_H17 cell
205 frequencies by *L. murinus* treatment compared to HSD feeding alone (Figure 4d-f). The effect
206 of HSD and concomitant *L. murinus* treatment on effector T cells was again largely specific to
207 T_H17, as a similar pattern was not observed for T_H1 markers. Except for the siLPL, HSD and
208 *L. murinus* treatment did not alter the expression of T_H1 cytokine IFN-γ (Extended Data Figure
209 9 h-j). In addition, the frequencies of regulatory CD4⁺CD25⁺ Foxp3⁺ T cells (T_{reg}) were neither
210 significantly affected by the HSD, nor by concomitant *L. murinus* treatment in intestinal and
211 splenic tissues (data not shown). Thus, *L. murinus* prevents HSD-induced generation of T_H17
212 cells and consequently ameliorates salt-sensitive hypertension.

213

214 **Salt challenge in healthy humans**

215 To corroborate our findings in humans, we conducted an exploratory pilot study in healthy
216 male volunteers, where participants were subjected to an increased salt intake for 14 days.
217 Participants received 6 g sodium chloride per day (corresponding to 2.36 Na⁺ g/day) using slow-
218 release NaCl tablets in addition to their accustomed diets. According to dietary records, salt
219 intake from foods and drinks was similar between baseline and day 14 of high salt. During high
220 salt challenge, the total salt intake was 13.8±2.6 g/day (Extended Data Figure 10a). We

221 monitored ambulatory blood pressure at baseline and after salt challenge in a subgroup of 8
222 participants. To standardize blood pressure measurements and exclude physical activity or
223 stress-driven alterations during daytime²⁸ unrelated to salt-sensitivity, we monitored nocturnal
224 blood pressure during bed rest. Compared to baseline, high salt challenge significantly
225 increased mean nocturnal systolic and diastolic blood pressure (Figure 5a). Since HSD
226 increased T_H17 cells in mice, we analyzed T_H17 cells in human blood before and after high salt.
227 Analysis of peripheral blood lymphocytes using flow cytometry revealed a significant increase
228 in CD4⁺IL-17A⁺TNF- α ⁺ T_H17 cells (Figure 5b).

229 To investigate the effect of high salt challenge on the human gut microbiome, we analyzed
230 the abundance of *Lactobacilli* in fecal samples before and after high salt challenge. To achieve
231 more detailed taxonomic resolution, full shotgun metagenomic was performed (see
232 Supplementary Information). *Lactobacillus* is not a dominant member of the human feces. In a
233 control data set used here^{29,30} only 41.3% were positive for any *Lactobacillus*. In our present
234 study, likewise 5 of 12 (41.7%) subjects were positive for at least one gut *Lactobacillus* species
235 at baseline (Figure 5c). Overall, we detected 7 different gut *Lactobacillus* species at baseline
236 (Figure 5c, species assignment using SpecI³¹). After high salt challenge, nine of ten initially
237 present *Lactobacillus* populations could no longer be detected in the respective study subjects,
238 suggesting a loss of *Lactobacillus* species (Supplementary Information and Extended Data
239 Figure 10b, c, d for cross-validation). To test whether this is expected for the human gut over
240 time, we reanalyzed 121 published Illumina-sequenced healthy gut metagenomes^{29,30} with time
241 course information. A Kaplan-Meier survival analysis on all *Lactobacillus* populations revealed
242 a significantly decreased survival (defined here as continued detectability) rate of *Lactobacillus*
243 gut populations under HSD (Figure 5d). Compared to non-*Lactobacillus* species, *Lactobacilli*
244 were lost significantly faster under HSD, reflecting high salt impact on an intrinsically low-
245 resilience taxon (Supplementary Information and Extended Data Figure 10e, f). Furthermore,
246 we observed that several study subjects had gained at least one novel *Lactobacillus* species by

247 day 14, which was not detected at baseline (Extended Data Fig. 10g-i). We speculate that this
248 is the consequence of ingested *Lactobacillus*-containing foods, since study participants were
249 not subjected to dietary restrictions. Thus, high salt challenge induces an increase in blood
250 pressure and T_H17 cells in healthy subjects, alongside reducing survival of intestinal
251 *Lactobacillus* species in subjects harboring *Lactobacillus* at baseline.

252

253 **Discussion**

254 Our data document the impact of an increased salt consumption on intestinal bacteria in mice
255 and men and broaden existing knowledge on the effects of this nutrient. Several intestinal
256 bacteria were affected by high salt; particularly *Lactobacillus spp.* were suppressed. In addition,
257 fecal metabolites levels, particularly bacterial tryptophan metabolites, responded to HSD in
258 mice. Such effects may contribute to salt-induced T_H17 responses and salt-sensitive conditions.
259 Since *L. murinus* produces ILA, we speculate that its salt-induced decrease with reduced ILA
260 generation could be responsible for an enhanced T_H17 response. Importantly, the experimental
261 approaches in mice demonstrate that *L. murinus* supplementation blunts HSD-induced T_H17
262 activation and ameliorates salt-sensitive hypertension and actively-induced EAE *in vivo*.
263 Yet, actively-induced EAE differs from spontaneous disease models¹⁴. It is thus currently
264 unclear whether high salt effects can be generalized beyond the actively-induced model and to
265 MS. These limitations may also extend to the recent controversy on more general effects of a
266 HSD in neuroinflammation^{32,33}. However, in the actively-induced EAE and hypertension
267 models used here and in humans, high salt enhanced T_H17 cells.

268 *Lactobacillus* metabolites are known to affect host physiology^{22,34} and ameliorate actively-
269 induced EAE²⁶. Other tryptophan metabolites have been shown to reduce blood pressure³⁵. Our
270 data in mice suggest that *L. murinus* may substantially influence the abundance of fecal
271 tryptophan metabolites, not excluding the possibility that other strains (e.g. *Bifidobacterium*
272 *spp.*) may be producers of similar importance. Additionally, we demonstrated that ILA inhibited

273 murine T_H17 polarization *in vitro*, a finding that needs to be addressed in more detail *in vivo*.
274 These results highlight the microbiome as a salt-sensitive compartment but do not speak against
275 a more direct effect of high salt on host cells. Earlier investigations showed that the ionic
276 microenvironment directly affects various immune cells³⁶⁻³⁹. Salt intake also has profound
277 actions on hormonal systems such as the renin-angiotensin-aldosterone axis.

278 Our exploratory pilot study in humans is limited in power and needs to be validated in larger
279 studies. Considering this limitation, it suggests that even a moderate salt challenge may affect
280 the persistence of intestinal *Lactobacilli* and other bacteria, along with an increase in pro-
281 inflammatory T_H17 cells and salt-sensitive blood pressure changes. Interestingly, newborn
282 infants have the greatest *Lactobacillus* abundance that decreases over time^{40,41}. Compared to
283 microbiomes from indigenous populations, *Lactobacillus* abundance in 'Western' gut
284 microbiomes is low⁴². Salt ingestion already starting at young age may partially have
285 contributed to the relative loss of *Lactobacilli* from Western microbiomes and thereby may play
286 role in the development of hypertension and autoimmunity.

287 Finally, the development of microbiota-targeted therapies is an intriguing new avenue for
288 many diseases. Nevertheless, changes in microbiome composition or function must first be
289 carefully shown to contribute to any disease. Our experimental data in mice suggest that the gut
290 microbiota might serve as a potential target to counteract salt-sensitive conditions. The
291 identification of *Lactobacillus* as a 'natural inhibitor' of high salt-induced T_H17 cells in mice
292 could serve as a basis for the development of novel prevention and treatment strategies. It is up
293 to randomized controlled trials in diseased humans to test this hypothesis. Moreover, any future
294 dietary salt intervention trial should thus consider monitoring the microbiome to expand on our
295 observations.

296 **References**

- 297 1 Manzel, A. *et al.* Role of "Western diet" in inflammatory autoimmune diseases. *Current*
298 *allergy and asthma reports* **14**, 404, doi:10.1007/s11882-013-0404-6 (2014).
- 299 2 O'Donnell, M. *et al.* Urinary sodium and potassium excretion, mortality, and
300 cardiovascular events. *The New England journal of medicine* **371**, 612-623,
301 doi:10.1056/NEJMoa1311889 (2014).
- 302 3 Weber, M. A. *et al.* Clinical practice guidelines for the management of hypertension in
303 the community a statement by the American Society of Hypertension and the
304 International Society of Hypertension. *Journal of hypertension* **32**, 3-15,
305 doi:10.1097/HJH.0000000000000065 (2014).
- 306 4 Taylor, J. 2013 ESH/ESC guidelines for the management of arterial hypertension.
307 *European heart journal* **34**, 2108-2109 (2013).
- 308 5 Mozaffarian, D. *et al.* Global sodium consumption and death from cardiovascular
309 causes. *The New England journal of medicine* **371**, 624-634,
310 doi:10.1056/NEJMoa1304127 (2014).
- 311 6 Coffman, T. M. Under pressure: the search for the essential mechanisms of
312 hypertension. *Nature medicine* **17**, 1402-1409, doi:10.1038/nm.2541 (2011).
- 313 7 Wenzel, U. *et al.* Immune Mechanisms in Arterial Hypertension. *Journal of the*
314 *American Society of Nephrology : JASN* **27**, 677-686, doi:10.1681/ASN.2015050562
315 (2016).
- 316 8 Guzik, T. J. *et al.* Role of the T cell in the genesis of angiotensin II induced hypertension
317 and vascular dysfunction. *The Journal of experimental medicine* **204**, 2449-2460,
318 doi:10.1084/jem.20070657 (2007).
- 319 9 Madhur, M. S. *et al.* Interleukin 17 promotes angiotensin II-induced hypertension and
320 vascular dysfunction. *Hypertension* **55**, 500-507,
321 doi:10.1161/HYPERTENSIONAHA.109.145094 (2010).

- 322 10 Norlander, A. E. *et al.* Interleukin-17A Regulates Renal Sodium Transporters and Renal
323 Injury in Angiotensin II-Induced Hypertension. *Hypertension* **68**, 167-174,
324 doi:10.1161/HYPERTENSIONAHA.116.07493 (2016).
- 325 11 Kleinewietfeld, M. *et al.* Sodium chloride drives autoimmune disease by the induction
326 of pathogenic TH17 cells. *Nature* **496**, 518-522, doi:10.1038/nature11868 (2013).
- 327 12 Wu, C. *et al.* Induction of pathogenic TH17 cells by inducible salt-sensing kinase SGK1.
328 *Nature* **496**, 513-517, doi:10.1038/nature11984 (2013).
- 329 13 Miossec, P., Korn, T. & Kuchroo, V. K. Interleukin-17 and type 17 helper T cells. *The*
330 *New England journal of medicine* **361**, 888-898, doi:10.1056/NEJMra0707449 (2009).
- 331 14 Bettelli, E. Building different mouse models for human MS. *Annals of the New York*
332 *Academy of Sciences* **1103**, 11-18, doi:10.1196/annals.1394.021 (2007).
- 333 15 David, L. A. *et al.* Diet rapidly and reproducibly alters the human gut microbiome.
334 *Nature* **505**, 559-563, doi:10.1038/nature12820 (2014).
- 335 16 Turnbaugh, P. J. *et al.* An obesity-associated gut microbiome with increased capacity
336 for energy harvest. *Nature* **444**, 1027-1031, doi:10.1038/nature05414 (2006).
- 337 17 Honda, K. & Littman, D. R. The microbiota in adaptive immune homeostasis and
338 disease. *Nature* **535**, 75-84, doi:10.1038/nature18848 (2016).
- 339 18 Ivanov, II *et al.* Induction of intestinal Th17 cells by segmented filamentous bacteria.
340 *Cell* **139**, 485-498, doi:10.1016/j.cell.2009.09.033 (2009).
- 341 19 Sun, Z. *et al.* Expanding the biotechnology potential of lactobacilli through comparative
342 genomics of 213 strains and associated genera. *Nature communications* **6**, 8322,
343 doi:10.1038/ncomms9322 (2015).
- 344 20 Wannemuehler, M. J., Overstreet, A. M., Ward, D. V. & Phillips, G. J. Draft genome
345 sequences of the altered schaedler flora, a defined bacterial community from gnotobiotic
346 mice. *Genome announcements* **2**, doi:10.1128/genomeA.00287-14 (2014).

- 347 21 Li, J. *et al.* An integrated catalog of reference genes in the human gut microbiome.
348 *Nature biotechnology* **32**, 834-841, doi:10.1038/nbt.2942 (2014).
- 349 22 Zelante, T. *et al.* Tryptophan catabolites from microbiota engage aryl hydrocarbon
350 receptor and balance mucosal reactivity via interleukin-22. *Immunity* **39**, 372-385,
351 doi:10.1016/j.immuni.2013.08.003 (2013).
- 352 23 Jangi, S. *et al.* Alterations of the human gut microbiome in multiple sclerosis. *Nature*
353 *communications* **7**, 12015, doi:10.1038/ncomms12015 (2016).
- 354 24 Berer, K. *et al.* Commensal microbiota and myelin autoantigen cooperate to trigger
355 autoimmune demyelination. *Nature* **479**, 538-541, doi:10.1038/nature10554 (2011).
- 356 25 Haghikia, A. *et al.* Dietary Fatty Acids Directly Impact Central Nervous System
357 Autoimmunity via the Small Intestine. *Immunity* **43**, 817-829,
358 doi:10.1016/j.immuni.2015.09.007 (2015).
- 359 26 Rothhammer, V. *et al.* Type I interferons and microbial metabolites of tryptophan
360 modulate astrocyte activity and central nervous system inflammation via the aryl
361 hydrocarbon receptor. *Nature medicine* **22**, 586-597, doi:10.1038/nm.4106 (2016).
- 362 27 Khalesi, S., Sun, J., Buys, N. & Jayasinghe, R. Effect of probiotics on blood pressure: a
363 systematic review and meta-analysis of randomized, controlled trials. *Hypertension* **64**,
364 897-903, doi:10.1161/HYPERTENSIONAHA.114.03469 (2014).
- 365 28 Hansen, T. W. *et al.* Predictive role of the nighttime blood pressure. *Hypertension* **57**,
366 3-10, doi:10.1161/HYPERTENSIONAHA.109.133900 (2011).
- 367 29 Forslund, K. *et al.* Country-specific antibiotic use practices impact the human gut
368 resistome. *Genome research* **23**, 1163-1169, doi:10.1101/gr.155465.113 (2013).
- 369 30 Voigt, A. Y. *et al.* Temporal and technical variability of human gut metagenomes.
370 *Genome biology* **16**, 73, doi:10.1186/s13059-015-0639-8 (2015).
- 371 31 Mende, D. R., Sunagawa, S., Zeller, G. & Bork, P. Accurate and universal delineation
372 of prokaryotic species. *Nature methods* **10**, 881-884, doi:10.1038/nmeth.2575 (2013).

- 373 32 Farez, M. F., Fiol, M. P., Gaitan, M. I., Quintana, F. J. & Correale, J. Sodium intake is
374 associated with increased disease activity in multiple sclerosis. *Journal of neurology,*
375 *neurosurgery, and psychiatry* **86**, 26-31, doi:10.1136/jnnp-2014-307928 (2015).
- 376 33 Fitzgerald, K. C. *et al.* Sodium intake and multiple sclerosis activity and progression in
377 BENEFIT. *Annals of neurology* **82**, 20-29, doi:10.1002/ana.24965 (2017).
- 378 34 Lamas, B. *et al.* CARD9 impacts colitis by altering gut microbiota metabolism of
379 tryptophan into aryl hydrocarbon receptor ligands. *Nature medicine* **22**, 598-605,
380 doi:10.1038/nm.4102 (2016).
- 381 35 Wang, Y. *et al.* Kynurenine is an endothelium-derived relaxing factor produced during
382 inflammation. *Nature medicine* **16**, 279-285, doi:10.1038/nm.2092 (2010).
- 383 36 Binger, K. J. *et al.* High salt reduces the activation of IL-4- and IL-13-stimulated
384 macrophages. *The Journal of clinical investigation* **125**, 4223-4238,
385 doi:10.1172/JCI80919 (2015).
- 386 37 Eil, R. *et al.* Ionic immune suppression within the tumour microenvironment limits T
387 cell effector function. *Nature* **537**, 539-543, doi:10.1038/nature19364 (2016).
- 388 38 Hernandez, A. L. *et al.* Sodium chloride inhibits the suppressive function of FOXP3+
389 regulatory T cells. *The Journal of clinical investigation* **125**, 4212-4222,
390 doi:10.1172/JCI81151 (2015).
- 391 39 Jantsch, J. *et al.* Cutaneous Na⁺ storage strengthens the antimicrobial barrier function
392 of the skin and boosts macrophage-driven host defense. *Cell metabolism* **21**, 493-501,
393 doi:10.1016/j.cmet.2015.02.003 (2015).
- 394 40 Cox, L. M. *et al.* Altering the intestinal microbiota during a critical developmental
395 window has lasting metabolic consequences. *Cell* **158**, 705-721,
396 doi:10.1016/j.cell.2014.05.052 (2014).

397 41 Tamburini, S., Shen, N., Wu, H. C. & Clemente, J. C. The microbiome in early life:
398 implications for health outcomes. *Nature medicine* **22**, 713-722, doi:10.1038/nm.4142
399 (2016).

400 42 Martinez, I. *et al.* The gut microbiota of rural papua new guineans: composition,
401 diversity patterns, and ecological processes. *Cell reports* **11**, 527-538,
402 doi:10.1016/j.celrep.2015.03.049 (2015).

403

404 **Extended Data Information** is available in the online version of the paper.

405

406 **Acknowledgements** We thank Gabriele N'diaye, Ilona Kamer, Silvia Seubert, Petra Voss,
407 Juliane Anders, Christiane Schmidt, Anneleen Geuzens, Rajna Hercog and Stefanie Kandels-
408 Lewis for assistance. We thank John J. Mullins and Friedrich C. Luft for their support. This
409 study was funded by grants from the German Centre for Cardiovascular Research (DZHK; BER
410 1.1 VD), the Center for Microbiome Informatics and Therapeutics, and the MetaCardis
411 consortium. D.N.M., J.J. and M.G. were supported by the German Research Foundation (DFG).
412 R.A.L. holds an endowed professorship supported by Novartis Pharma. M.K. was supported by
413 the European Research Council (ERC) under the European Union's Horizon 2020 research and
414 innovation program (640116), by a SALK-grant from the government of Flanders, Belgium and
415 by an Odysseus-grant of the Research Foundation Flanders (FWO), Belgium. *L. reuteri* was
416 kindly provided by L. Romani.

417

418 **Author Contributions** N.W. led and conceived the project, designed and performed most
419 experiments, analyzed and interpreted the data. M.G.M., S.W.O., S.M.K. performed 16S
420 sequencing and data analysis. S.J., D.T., M.Ba., C.W. performed animal experiments and
421 analyzed data. H.B., S.J., A.B., D.A.G., B.F.C. performed and analyzed flow cytometry. Li.Ma.,
422 S.M.K., V.S., P.N., R.G.G. performed bacterial growth experiments. O.V., C.F. performed

423 metabolite analysis with input by A.B. and M.G.M. La.M., F.H.K. and L.K. performed 16S
424 qPCR. N.R. performed sodium analyses. K.F. performed metagenomic analyses with
425 contributions by P.I.C. and S.S. M.Bo., R.D. and A.M. conducted the clinical study. A.K.
426 performed statistical analyses. M.G., A.T., J.M.T, S.K., P.B., J.J. supervised the experiments
427 and analyses. D.N.M., E.J.A., M.K. and R.A.L. conceived the project, supervised the
428 experiments and interpreted the data. N.W. and D.N.M. wrote the manuscript with key editing
429 by E.J.A., R.A.L., M.K., K.F. and further input from all authors.

430

431 **Author Information** The authors declare no competing financial interests. Correspondence
432 and requests for materials should be addressed to dominik.mueller@mdc-berlin.de and
433 ejalm@mit.edu.

434 **Figure legends**

435

436 **Figure 1. HSD alters the fecal microbiome and depletes *Lactobacillus* in mice.** (a) AdaBoost
437 identified eight 16S rDNA OTUs distinguishing NSD from HSD samples. (b) Classifier
438 accuracy per mouse and diet. (c) Relative OTU abundances on HSD day 14 ($n=12$ mice, $n=8$
439 NSD control mice). (d) *Lactobacillus* abundance over time. Samples $>1\%$ not shown. Boxplots:
440 IQR, whiskers $1.5 \times \text{IQR}$. (e, f) *L. murinus* qPCR ($n=8$ mice). $**p < 0.01$, $***p < 0.001$ paired two-
441 tailed t -test. (g) Fecal indole-3-lactic acid (ILA), $n=12$ mice per group. $*p < 0.05$, Wilcoxon
442 signed-rank test. (h) Fecal ILA in gnotobiotic mice ($n=8$ germ-free, $n=7$ *L. murinus*-
443 monocolonized mice). $****p < 0.0001$ unpaired two-tailed t -test.

444

445 **Figure 2. *L. murinus* prevents HSD-induced exacerbation of EAE and reduces T_H17 cells.**

446 (a) Mean disease scores \pm s.e.m. of MOG₃₅₋₅₅-EAE mice fed NSD ($n=9$), HSD ($n=11$), or HSD
447 with *L. murinus* ($n=6$). (b) siLPL (day 3 p.i.) analyzed for $CD4^+ IL-17A^+ IFN-\gamma$ cells ($n=4$). (c,
448 d) Spleens ($n=5$) and spinal cords (NSD $n=4$; HSD $n=6$; HSD+*L. murinus* $n=5$, day 17 p.i.)
449 were similarly analyzed. Representative plots, quantification to the right. Mean \pm s.e.m., circles
450 represent individual mice. $*p < 0.05$, $**p < 0.01$ by one-way ANOVA and post-hoc Tukey's for
451 (c), Kruskal-Wallis and Dunn's post-hoc test for (a, b, d). n equals mice per group.

452

453 **Figure 3. Putative role for ILA.** (a) HSD reduces fecal ILA in MOG₃₅₋₅₅-EAE mice ($n=5$),
454 day 10 p.i. (b) Fecal ILA in HSD+*L. murinus* treated ($n=6$) vs. HSD-fed MOG₃₅₋₅₅-EAE mice
455 ($n=8$), day 10 p.i. Circles represent samples from individual mice. $*p < 0.05$ using unpaired one-
456 tailed t -test for (a); Mann-Whitney U test for (b). (c) Naïve murine $CD4^+$ T cells cultured under
457 T_H17 -polarizing conditions in presence (+ILA) or absence (+vehicle) of ILA, analyzed for IL-
458 17A ($n=3$ replicates per group, mean \pm s.e.m., one representative out of two independent

459 experiments is shown). *** $p < 0.001$ vs. vehicle using one-way ANOVA and Tukey's post-hoc
460 test.

461

462 **Figure 4. *L. murinus* ameliorates salt-sensitive hypertension and reduces T_H17 cells.**

463 Continuous blood pressure recordings in $n=7$ FVB/N mice. (a) Mean systolic pressures over

464 time and (b) systolic and diastolic pressures as boxplots (IQR, whiskers $1.5 \times \text{IQR}$). ### $p < 0.001$

465 vs. NSD, *** $p < 0.001$ vs. HSD (linear mixed model). (c) $CD4^+ROR\gamma^+$ siLPL in mice fed NSD

466 ($n=7$), HSD ($n=8$) or HSD+*L. murinus* ($n=9$). (d-f) $CD4^+IL-17A^+IFN-\gamma^-$ siLPL, cLPL,

467 splenocytes in mice fed NSD ($n=5$), HSD ($n=6$; siLPL $n=7$) and HSD+*L. murinus* ($n=6$; siLPL

468 $n=5$). Representative plots per group, quantification showing mean \pm s.e.m., circles represent

469 individual mice. * $p < 0.05$, ** $p < 0.01$, one-way ANOVA and post-hoc Tukey's (c, e, f), Kruskal-

470 Wallis and post-hoc Dunn's (d).

471

472 **Figure 5. High salt challenge affects blood pressure, T_H17 cells and *Lactobacilli* in healthy**

473 **humans.** (a) Mean nocturnal systolic and diastolic blood pressures and (b) $IL-17A^+TNF-\alpha^+$

474 cells in $CD4^+$ enriched PBMC (one representative subject is shown) in $n=8$ males at baseline

475 and after challenge. * $p < 0.05$, ** $p < 0.01$, **** $p < 0.0001$, paired one-tailed *t*-test (a) and

476 Wilcoxon signed-rank test (b). (c) Loss of *Lactobacilli* after high salt challenge. Subjects

477 positive for *Lactobacilli* at baseline are shown. Split cells show abundance at baseline (left) and

478 after high salt (right), crosses indicate nondetection. (d) Kaplan-Meier curves comparing the

479 persistence of *Lactobacilli* to control cohorts (log-rank test).

480

481 **Methods**

482

483 **Animal ethics**

484 All animal experiments were conducted in accordance with institutional, state and federal
485 guidelines and with permission of the local animal ethics committees (Landesamt für
486 Gesundheit und Soziales Berlin, Germany; Regierung Unterfranken, Würzburg, Germany;
487 Ethical Committee for Animal Experiments, Hasselt University, Belgium). Male mice were
488 maintained on a 12:12 hour day:night cycle with constant access to food and water.

489

490 **Mouse high salt feeding and feces collection**

491 All normal salt (NSD, E15430-047) and high salt (HSD, E15431-34) purified diets used for
492 mouse experiments were purchased from Ssniff (Soest, Germany). Diets were gamma-
493 irradiated (25kGy) and identical in composition except for NaCl content (NSD: 0.5% NaCl,
494 HSD: 4% NaCl). Drinking water for HSD animals was supplemented with 1% NaCl.

495 For fecal microbiome analyses, male FVB/N mice aged 12 weeks were purchased from Charles
496 River and accustomed to NSD. Control animals remained on the NSD (n=8), others were
497 switched to HSD (n=12) for 14 days. A subgroup was switched back to NSD for another 14
498 days (n=8). Body weight and food intake were monitored. To avoid cage effects, mice were
499 housed individually. Fresh fecal pellets were collected directly from the anal orifices,
500 immediately shock-frozen in liquid nitrogen and stored at -80°C for later analyses.

501

502 **DNA extraction from mouse feces and 16S sequencing**

503 DNA was extracted from a single fecal pellet from each mouse using the Power Soil kit (MO
504 BIO Laboratories, Carlsbad, CA, USA). The protocol was modified from the manufacturer's
505 instructions to include proteinase K treatment to further lyse cells. After addition of proteinase
506 K (final concentration 5 mg/ml) samples were incubated at 65 °C for 10 min and further 10 min

507 at 95 °C. Plates were inverted to mix during both incubations. The V4 region of the 16S rRNA
508 gene was amplified with 515F and 806R primers⁴³ using a two-step PCR library preparation as
509 previously described⁴⁴. An Illumina MiSeq was run for 250 cycles to produce paired-end reads.

510

511 **16S rDNA data processing**

512 The raw sequences were de-multiplexed, allowing at most 2 mismatches in the barcode before
513 discarding a sequence. Primers sequences were removed, allowing at most 2 mismatches in the
514 primer sequence before discarding a sequence. Forward and reverse reads were merged by
515 comparing alignments with lengths of 253±5 nucleotides. The alignment with the fewest
516 mismatches was used unless the number of mismatches was greater than 2, in which case the
517 read pair was discarded. Merged reads were filtered for quality by removing reads with more
518 than 2.0 expected errors⁴⁵. Each unique sequence was assigned a taxonomy using RDP⁴⁶,
519 truncating the taxonomy to the highest taxonomic level with at least 80% support. Sequences
520 that were assigned the same taxonomy were then placed in the same operational taxonomic unit
521 (OTU). *De novo* OTUs were also called using usearch⁴⁷.

522

523 **16S rDNA data analysis**

524 For most analyses, three samples were excluded because their read counts were low (< 1000
525 counts). The MDS ordination and PERMANOVA test were computed using R's vegan
526 package⁴⁸. The phylogenetic tree was generated from a single medoid sequence from each
527 OTU. Medoid sequences were selected by aligning all the sequences in each OTU with
528 PyNAST⁴⁹, computing a distance matrix with Clustal Omega⁵⁰, and selecting the medoid
529 sequence. Aligned sequences with at least 10 reads in their corresponding OTU were assembled
530 into a tree with FastTree 2.0⁵¹ and visualized with R's ape package⁵². The AdaBoost classifier⁵³
531 was run with 10⁷ estimators using Python's scikit-learn module⁵⁴. The random forest classifier⁵⁵
532 was run with 10⁶ estimators also using Python's scikit-learn module.

533

534 **Fecal metabolite analysis**

535 An extraction mixture of methanol-chloroform-water (MCW) (5:2:1/v:v:v) (Methanol LC-MS-
536 grade, Chloroform Reagent Plus ® 99,8% Sigma-Aldrich) with cinnamic acid (2 µg/ml, Sigma-
537 Aldrich) as internal standard was added to the sample. Samples were dissolved in MCW (1 ml/
538 60 mg of sample) using the tissue lyser (Precellys 24 lysis and homogenization, Bertin
539 Technologies, France), samples were cooled on ice between the shaking cycles. Samples were
540 shaken at 1,000 rpm and 4°C for 60 min. After addition of ice cold water (half of MCW volume)
541 samples were shaken at 1,000 rpm and 4°C for 10 min. Samples were centrifuged for 10 min at
542 14,000 rpm to separate the polar (top), lipid (bottom) and interface (tissue debris) layers. Polar
543 phase containing metabolites was dried under vacuum for 12 h.

544 Samples were derivatized as follows: the dried extracts were dissolved in 20 µl of
545 methoxyamine hydrochloride solution (Sigma, 40 mg/ml in pyridine (Roth)) and incubated for
546 90 min at 30°C shaken at 1,000 rpm followed by the addition of 40 µl of N-methyl-N-
547 [trimethylsilyl]trifluoroacetamide (MSTFA; Machery-Nagel, Dueren, Germany) and
548 incubation at 37°C for 45 min agitated at 1,000 rpm. The extracts were centrifuged for 10 min
549 at 14,000 rpm, and aliquots of 30 µl were transferred into glass vials (Chromacol, UK) for gas
550 chromatography-mass spectrometry (GC-MS) measurement. Metabolite analyses was
551 performed with a Pegasus IV mass-spectrometer (LECO, St. Joseph, USA) as described
552 previously⁵⁶. The GC-MS chromatograms were pre-processed with the ChromaTOF software
553 (LECO). Calculation of retention index, mass spectra identification and metabolite
554 quantification were performed using the in house Maui-SILVIA Software tool⁵⁷.

555 Measured values from 66 metabolites were obtained. Since a paired analysis (metabolites at
556 NSD baseline vs. metabolites after HSD) was performed, absence of a given value made the
557 exclusion of the corresponding second value necessary. This was in only 33 of 1056 cases
558 (3.1%). A small pseudocount value (0.001) was added to all metabolite values and data was

559 log₁₀ transformed. Data from each metabolite was normalized by subtracting the minimum and
560 dividing by the maximum value across all eight mice. The PCA was performed using the Python
561 scikit-learn package's PCA module. The heatmap was prepared with the Seaborn package's
562 clustermap function.

563

564 **Measurement of tryptophan metabolites**

565 Fecal pellets derived from mice were processed as previously described²². Chemicals used were
566 purchased from Sigma-Aldrich and were liquid chromatography (LC)-MS grade. Pellets were
567 diluted in 300 µl/10 mg feces 0.2 M acetate buffer (pH 4.2) and shaken with 1.5 ml methyl *tert*-
568 buthyl ether (MTBE) on a shaker at room temperature at 1,400 rpm for 10 min in the presence
569 of ceramic beads (2.8 mm Precellys Ceramic Beads, Peqlab). Samples were afterwards
570 centrifuged at 4°C at 9000×g. From the organic phase 1 ml was transferred into a new
571 Eppendorf vial and samples were concentrated using Eppendorf Concentrator 5301.
572 Concentrated samples were dissolved in 200 µl acetonitrile:H₂O 1:4 v/v containing 0.2%
573 formic acid and stored at -20°C for further analysis.

574 LC-MS/MS analysis was performed using an Agilent 1290 Infinity II UPLC system coupled to
575 an Agilent 6495 Triple Quad mass spectrometer equipped with an iFunnel ESI ion source
576 operated in the positive mode (Agilent Technologies, Santa Clara, CA, USA). The UPLC
577 column used was an Agilent Eclipse plus (100 mm × 2.1 mm, 1.8 µm). Chromatography was
578 performed under gradient conditions using mobile phase A (0.1% formic acid in water) and B
579 (0.1% formic acid in methanol). Gradient was started at 5% methanol, increased to 95% after
580 10 min with a constant flow rate of 0.3 ml/min during a total run time of 17 min. The column
581 temperature was set to 30°C. The injection volume was 1 µl. Drying gas was adjusted at
582 130°C/17 l/min, sheath gas at 400°C/11 l/min. Capillary and nozzle voltage were optimized at
583 3,500 V and 800 V, respectively. Analytes were monitored in the multiple reaction monitoring
584 mode. The optimal transitions, collision energies and cell accelerator voltages for each

585 compound were determined as in the following ILA m/z 206 -> 118 CE: 24V CAV: 1V; ICA
586 m/z 146 -> 118 CE: 13V CAV: 5V; IAA m/z 176 -> 130 CE: 17V CAV: 1V. Calibration curves
587 for the quantification of individual metabolites were established based on the changes in the
588 relative peak area in response to different target compound concentration. Linearity was $r^2 >$
589 0.99 over a range from 0.05 to 300 ng/ml for any compound.

590

591 **Isolation of *L. murinus***

592 Fecal samples from healthy male NSD-fed FVB/N mice were dissolved and diluted at a 1:10
593 dilution in anaerobic PBS (pH 7.6) containing L-cysteine HCl at 0.1% in a Coy Anaerobic
594 Chamber (5% H₂, 20% CO₂, 75% N₂). Samples were diluted 10-fold and each dilution spread
595 on LAMVAB agar⁵⁸. Plates were incubated at 37°C under anaerobic conditions and examined
596 for growth at 24 hours. Individual colonies growing at the highest dilution were picked into
597 LAMVAB medium and grown for an additional 16 hours. Liquid cultures were stored in 15%
598 DMSO. For identification of isolates, DNA was extracted by adding 5 µl liquid culture to 20 µl
599 sterile distilled water and storing at 4°C overnight; 2 µl of this extract was amplified with
600 Phusion HF polymerase in a 20 µl reaction using universal 16S primers 27F (5'-
601 AGAGTTTGATCMTGGCTCAG-3') and 1492R (5'-TACGGYTACCTTGTTACGACTT-
602 3'). PCR products were purified using Agencourt AMPure XP and submitted with the 27F
603 primer for Sanger sequencing. An isolate whose full-length 16S sequence shared 100% identity
604 with the V4-V5 region of the *Lactobacillus* species identified in the 16S library was selected
605 for further study. Frozen stocks of *L. murinus* (in PBS + 25% glycerol) were prepared, stored
606 at -80°C and used for gavage of salt-sensitive and EAE mice.

607

608 **Salt tolerance of *L. murinus* and selected gut commensals**

609 Frozen stocks of *L. murinus* were streaked onto MRS agar and incubated at 37°C under aerobic
610 conditions for 24 hours. Single colonies were picked into MRS medium and grown until mid-

611 log phase ($OD_{600} = 0.4-0.6$), at which time liquid cultures were diluted 1:100 into MRS medium
612 containing NaCl in the range of 0 to 2 OsM. In separate experiments, *E. coli* and *L. murinus*
613 were picked into LB (*E. coli*) or MRS (*L. murinus*) medium, respectively. Na^+ concentration of
614 growth media was determined using atomic absorption spectrometry or calculated. OD_{600} of
615 cultures was measured following 12-16 additional hours of growth. For comparison of the salt
616 tolerance of phylogenetically distinct gut commensals, *C. difficile* ATCC 700057, *A.*
617 *muciniphila* DSM 26127, and *P. excrementihominis* DSM 21040 were cultured under the same
618 conditions. Frozen stocks of each strain, along with *L. murinus*, were streaked onto Brucella
619 Blood Agar with vitamin K and hematin, and grown at 37°C in a Coy Anaerobic Chamber for
620 24 hours. Individual colonies were transferred into liquid Gifu anaerobic medium supplemented
621 with 0.25% porcine gastric mucin (Sigma) and grown until mid-log phase, at which time they
622 were diluted 1:100 into MGAM containing NaCl with concentrations of Na^+ ranging from 0.08
623 to 1.8 M. OD_{600} of cultures was measured after 48 hours of growth (to compensate for the slow
624 growth rates of some of the strains).

625

626 ***In vitro* growth of human-associated *Lactobacillus* isolates**

627 Human-associated *Lactobacillus* isolates were obtained from the German Culture Collection
628 (DSMZ, Braunschweig, Germany): *L. salivarius* (DSM-No. 20555), *L. ruminis* (DSM-No.
629 20403), *L. delbrueckii* subsp. *Delbrueckii* (DSM-No. 20074), *L. fermentum* (DSM-No. 20052).
630 *L. acidophilus* NCFM, *L. paracasei* (ATCC SD5275). *Lactobacillus* strains were grown
631 anaerobically in a gas chamber (Coy Laboratory Products, USA; 12% CO_2 , 2,5-5 % H_2 , and
632 83-85,5% N_2) in Gifu Anaerobic Medium Broth (MGAM) at 37°C. Overnight cultures were
633 diluted to an initial OD of 0.01 and growth was assessed in the presence of increasing
634 concentrations of NaCl by monitoring the absorbance at 578 nm using an Eon (Biotek)
635 microplate spectrophotometer in 30-minute intervals after 30 s of shaking. AUCs were

636 calculated using the trapezoidal rule and normalized to the AUC calculated for growth in
637 MGAM without addition of NaCl.

638

639 **Germ-free mice and *L. murinus* monocolonization**

640 C57BL/6J male mice were bred under germ-free conditions and kept under a 12-hour light cycle
641 and fed sterile NSD (E15430-047, Ssniff, Soest, Germany) *ad libitum*. For monocolonization,
642 mice were gavaged with 200 µl of *L. murinus* stock solution (10^7 CFU/ml, as described above)
643 and further maintained under sterile conditions for two weeks. Fecal pellets were harvested
644 under sterile conditions and immediately frozen in liquid nitrogen, or cultured in liquid
645 thioglycolate medium (bioMerieux), incubated for 7 days, streaked on sheep blood agar plates
646 (oxid, 24 hours) and further analyzed for species identification using MALDI-TOF (analyzed
647 by GIMmbH, Michendorf, Germany) as described previously⁵⁹.

648

649 **Salt-sensitive hypertension in mice**

650 To induce salt-sensitive hypertension, the L-NAME/salt mouse model was used as described
651 previously⁶⁰. This non-surgical intervention closely recapitulates salt-sensitive hypertension
652 common in humans⁶⁰. In brief, NSD-fed male FVB/N mice, aged 10-12 weeks, received
653 pretreatment with (L-NAME, 0.5 mg/ml, Sigma-Aldrich) via drinking water for 3 weeks,
654 followed by a 1-week washout period with NSD and normal drinking water. Then, mice were
655 switched to either HSD with oral administration of *L. murinus* (daily gavage of 200 µl 10^7
656 CFU/ml *L. murinus* suspension,), HSD with oral administration of control solution (daily
657 gavage of 200 µl PBS/glycerol) or NSD for two weeks. For blood pressure measurements, mice
658 were implanted with miniature subcutaneous radiotelemetry devices in anesthesia (Data
659 Sciences International, New Brighton, MN, USA) prior to the L-NAME/salt protocol. Thereby,
660 systolic and diastolic blood pressures were recorded continuously at 5 minute intervals in freely
661 moving mice. Following hypertension induction with HSD for 3 weeks, HSD was continued

662 and mice were concomitantly gavaged with 200 μ l 10^7 CFU/ml *L. murinus* in phosphate-
663 buffered saline (PBS) + glycerol daily. *L. reuteri* and *E. coli* Nissle 1917 were used for separate
664 experiments in a similar manner (10^7 CFU/ml in PBS + glycerol daily).

665 Mice were euthanized in anaesthesia, spleens and intestines were harvested. Single-cell
666 suspensions of small intestinal (si) and colonic (c) lamina propria lymphocytes (LPL) were
667 obtained by enzymatic and mechanical dissociation using the Lamina Propria Dissociation Kit
668 Mouse (Miltenyi Biotec, Bergisch Gladbach, Germany) according to the manufacturers'
669 protocol. Cell debris was removed using Percoll (GE Healthcare) density gradient
670 centrifugation as described previously⁶¹. Splenocyte single-cell suspensions were obtained
671 using 70 μ m strainers, followed by erythrocyte lysis and subsequent filtering using a 40 μ m
672 mesh. Cells were counted by trypan blue exclusion and labeled for flow cytometric analysis.

673 Isolated immune cells were either directly stained for surface markers using the respective
674 fluorochrome-conjugated antibodies (30 min in PBS supplemented with EDTA and BSA) or
675 restimulated with 50 ng/ml phorbol-12-myristate-13-acetate (PMA, Sigma-Aldrich), 750 ng/ml
676 ionomycin (Sigma Aldrich) and 0.75 μ l/ml GolgiStop (BD Bioscience) for 4h at 37°C and 5%
677 CO₂ in RPMI 1640 medium (Sigma) supplemented with 10% FBS, 1% penicillin/streptomycin.
678 For all measurements, dead cell exclusion was performed using fixable viability dye for 405nm
679 (Thermo Fisher). For intracellular staining, cells were permabilized and fixed using the FoxP3
680 Staining Buffer Kit (eBioscience) and labeled using the respective antibodies. Antibodies used
681 are listed below. Cells were analyzed with the BD FACSCanto II flow cytometer and BD
682 FACSDiva software (BD Bioscience). Data analysis was performed with FlowJo v10 (FlowJo
683 LLC, Ashland, Oregon, USA).

684

685 **Experimental autoimmune encephalomyelitis (EAE)**

686 Male C57BL/6J mice (Charles River), aged 10-12 weeks, were either fed a NSD, a HSD (Ssniff,
687 as described above) with oral administration of *L. murinus* or *L. reuteri* (daily gavage of 200 μ l

688 10⁷ CFU/ml suspension) or a HSD with oral administration of solvent (daily gavage of 200 µl
689 PBS/glycerol). EAE was induced as described previously¹¹. Briefly, mice were anaesthetized
690 and subcutaneously injected with 200 µg MOG₃₅₋₅₅ and 200 µg CFA. Pertussis toxin (200
691 ng/mouse) was applied intraperitoneally on days 0 and 2 post immunization (p.i.). Clinical
692 symptoms were assessed daily according to a 5-point scale ranging from 0 (no symptoms) to 5
693 (moribund)¹¹. For disease courses, only mice with clinical symptoms were included.

694 On day 17 p.i., mice were euthanized in anesthesia and CNS tissue was harvested, disrupted
695 with a 5 ml glass homogenizer and strained through a 100 µm cell-strainer. CNS cell suspension
696 was resuspended in 6 ml 30% isotonic Percoll (GE Healthcare) for a three-step density gradient.
697 Lymphocytes were harvested from the interphases, washed and further analyzed by flow
698 cytometry. Spleens were disrupted with a glass homogenizer, filtered through a 100-µm cell
699 strainer and treated with 0.14 M ammonium chloride to lyse erythrocytes. To analyze the early
700 inflammatory response in the small intestine, a subset of mice was euthanized on day 3 p.i. and
701 the small intestine was harvested and processed as described above to obtain LPL.

702 In two additional experimental setups EAE was induced in male germ-free (GF) C57BL/6J
703 mice fed gamma-sterilized (50 Gy) NSD or HSD diets. First, GF mice were either fed NSD or
704 HSD (2 weeks prior to immunization and thereafter). Second, GF mice were fed NSD and either
705 monocolonized with SFB (by introduction of feces from SFB monocolonized mice) or SFB and
706 *L. murinus*. In both experimental subgroups intestines were harvested on day 3 p.i. for flow
707 cytometry analyses.

708 Single-cell suspensions were analyzed by staining for extra- and intracellular markers. Dead
709 cells were excluded by a fixable viability dye eFluor780 (eBioscience), Fc-block was performed
710 using anti-CD16/32 antibody (eBioscience). For intracellular cytokine staining, cells were
711 stimulated with ionomycin (1 µM) and PMA (50 ng/ml) in the presence of monensin (2 µM)
712 for 4 hours. Cells were stained for surface markers with the respective fluorochrome-conjugated
713 antibodies for 30 min and permeabilized using Fixation and Permeabilization Buffer

714 (eBioscience) according to the manufacturer's protocol. Intracellular cytokines were labeled
715 with the respective fluorochrome-conjugated antibodies for 30-45 min. For antibodies used see
716 below. Cells were analyzed with the BD FACSCanto II flow cytometer and BD FACSDiva
717 software (BD Bioscience). Data analysis was performed with FlowJo (LLC).

718 For quantitative real-time PCR, tissue was homogenized in 500 µl peqGOLD TriFast with an
719 Ultra-Turrax for 30 s followed by total RNA isolation with PerfectBind RNA Columns
720 (peqGOLD HP Total RNA Kit, Peqlab). RNA yield was quantified by absorbance
721 measurements at 260 nm and reversely transcribed into cDNA using QuantiTect transcriptase
722 (Qiagen). PCR reactions were performed at a 5 µl scale on a qTower real-time PCR System
723 (Analytic Jena, Germany) in triplicates using Taqman Assays (Thermo Fisher) for *Il17a*
724 (Mm00439618_m1), *Rorc* (Mm01261019_g1) and *Csf2* (Mm01290062_m1). Relative
725 quantification was performed by the $\Delta\Delta CT$ method, normalizing target gene expression on
726 *Actb*/ β -Actin (Mm00607939_s1) as housekeeping gene.

727

728 **Antibodies used for flow cytometry of murine cells**

729 Anti-CD3 ϵ -FITC and anti-CD3 ϵ -VioBlue (clone 17A2, Miltenyi), anti-CD4-APC-Vio770
730 (clone GK1.5, Miltenyi), anti-CD4-Pacific Blue and anti-CD4-FITC (clone RM4-5, BD), anti-
731 CD25-VioBlue and anti-CD25-FITC (clone 7D4, Miltenyi), anti-FoxP3-PerCP-Cy5.5 (clone
732 FJK-16s, eBioscience), anti-IFN- γ -PE-Cy7 and anti-IFN- γ -APC (clone XMG1.2, eBioscience),
733 anti-IL-17A-PE (clone eBio17B7, eBioscience), anti-ROR γ t-APC (clone REA278, Miltenyi).

734

735 **Electrolyte analysis of mouse feces**

736 Fecal samples from NSD- and HSD-fed mice were collected and stored at -80°C until further
737 analysis. n=7-9 feces samples were pooled, weighed and then processed as described
738 previously⁶². In brief, samples were weighted, desiccated, ashed, dissolved and measured for
739 Na⁺ concentration by atomic adsorption spectrometry (Model 3100, Perkin Elmer).

740

741 **Measurement of intestinal transit**

742 Male FVB/N mice were fed NSD or HSD for 14 days. Mice were administered activated
743 charcoal (0.5 g/10 ml in 0.5% methylcellulose; 0.1 ml/10g body weight by oral gavage). Twenty
744 min later mice were euthanized and the distance travelled by charcoal was measured.

745

746 **High salt challenge study in healthy humans**

747 We performed an open-label clinical pilot study to investigate the effect of an increased salt
748 intake on cardiovascular and immunoregulatory functions in healthy men (ClinicalTrials.gov
749 identifier: NCT02509962). The study was conducted at the Experimental and Clinical Research
750 Center Berlin (ECRC), Germany, in accordance with the ethical standards of the institutional
751 review board. The institutional review board of Charité University Medicine Berlin approved
752 the study (EA1/138/15) and written informed consent was obtained from all participants prior
753 to study entry. Key inclusion criteria were men, aged 18-50 years and a body mass index
754 between 18.5 and 29.9 kg/m². Key exclusion criteria were any cardiovascular, metabolic
755 (diabetes), autoimmune, liver and kidney diseases, alcohol or drug abuse. To increase salt
756 intake, subjects (n=12, included until March 2016, for baseline characteristics see
757 Supplementary Information) received 10 coated tablets daily (three with breakfast, three with
758 lunch and four with dinner) for two weeks, each tablet containing 600 mg sodium chloride in a
759 slow release formulation (Slow Sodium Tablets, HK Pharma Ltd., Bedford, UK), yielding an
760 increase of habitual salt intake by 6 g/d. Subjects were asked not to change their dietary habits
761 during the study. Sodium intake from ingested foods and drinks was calculated from dietary
762 records of three consecutive days using OptiDiet Plus software 5.1.2 (GOE mbH, Linden,
763 Germany), a professional analysis software that is based on nutritional content of food as
764 provided by the German Nutrient Database⁶³.

765 Stool samples were collected at baseline and on day 13 of the high salt challenge from all 12
766 subjects. Briefly, subjects collected fresh fecal samples using disposable toilet seat covers
767 (Süsse Labortechnik, Gudensberg, Germany) and plastic vessels with spatula (Sarstedt AG,
768 Nümbrecht, Germany). Closed vessels with fecal samples were immediately frozen in a
769 domestic freezer at -20°C and subsequently transferred to the study center on dry ice, where
770 samples were stored at -80°C until further use.

771 At baseline and on day 13 of the high salt challenge, 8 subjects received ambulatory blood
772 pressure monitors (ABPM, Mobil-O-Graph, I.E.M. GmbH, Stolberg, Germany) for nocturnal
773 blood pressure monitoring (measurements at bed rest every 30 min, subjects indicated bed rest
774 by pressing the day/night button of the ABPM).

775 Venous blood was taken at baseline and on day 14 of the HSD for immediate isolation of
776 peripheral blood mononuclear cells (PBMC).

777

778 **Metagenomic sequencing of human fecal samples**

779 Samples were processed, extracted and sequenced as per the procedure in Voigt et al.³⁰ with
780 SpecI³¹ and mOTU⁶⁴ taxonomic abundances estimated using MOCAT⁶⁵. Since *Lactobacillus*
781 is low-abundance in the human gut, to verify results are robust to changes in the bioinformatic
782 protocol, samples were additionally processed using the complementary tool MetaPhlan⁶⁶
783 which uses lineage-specific marker genes as opposed to the universal marker genes informing
784 SpecI and mOTU species quantification, with MetaPhlan species detection results almost
785 identical to mOTU species detection results (Extended Data Figure 10a, b).

786 Previously published healthy human gut shotgun metagenomes where multiple samples from
787 the same individual at different time points were available were taken from Voigt et al.³⁰ and
788 from the Human Microbiome Project (2012, processed as described in Forslund et al.²⁹).
789 Survival analysis was done using the R 'survival' package⁶⁷ as outlined by Therneau &
790 Grambsch⁶⁸.

791

792 **Human blood cell analysis**

793 Peripheral venous blood was obtained from study participants. Peripheral blood mononuclear
794 cells (PBMCs) were immediately isolated by density centrifugation using Biocoll (Merck,
795 Darmstadt, Germany). 10^6 CD4⁺ enriched cell fractions isolated by CD4⁺ T Cell Kit (Miltenyi)
796 were plated onto U-bottom plates and were restimulated for 4 hours at 37°C, 5% CO₂ in a
797 humidified incubator. Restimulation was conducted in a final volume of 200 µl RPMI 1640
798 (Sigma) supplemented with 10% FBS (Merck), 100 U/ml penicillin (Sigma), 100 mg/ml
799 streptomycin (Sigma), 50 ng/ml PMA (Sigma), 250 ng/ml ionomycin (Sigma) and 1.3 µl/ml
800 Golgistop (BD). After restimulation cells were stained with Life/Dead Fixable Aqua Dead cell
801 kit (Thermo Fisher) and monoclonal CD3-PerCP-Vio700 antibody (clone BW264/56,
802 Miltenyi). Cells were fixed and permeabilized with Foxp3/Transcription Factor Staining Buffer
803 kit (eBioscience) and labeled using anti-IL-17A-APC-Vio770 (clone CZ8-2361, Miltenyi) and
804 anti-TNF- α -eFlour 450 (clone Mab11, eBioscience) monoclonal antibodies. Cells were
805 analyzed using a FACSCanto II flow cytometer and FACSDiva software (BD). Data analysis
806 was performed with FlowJo (LLC).

807

808 **Murine T_H17 cell polarization**

809 Splenic T cells were isolated by magnetic activated cell sorting using the “Pan T cell isolation
810 kit II” (Miltenyi Biotec) according to the manufacturer’s instructions. Isolated T cells were
811 collected and re-suspended in MACS buffer at $3 \cdot 10^7$ cells/ml. For APC free differentiation,
812 cells were fluorescently stained for 30 min in an antibody cocktail containing anti-CD4-FITC
813 (RM4-5, eBioscience), anti-CD44-PE (IM7, BioLegend), anti-CD62L-APC (MEL-14,
814 eBioscience) and anti-CD25-PE-Cy5 (PC61.5, eBioscience) and subsequently purified by
815 fluorescence activated cell sorting on MoFlo (Beckman-Coulter). Sorted naive T cells
816 (CD4⁺CD62L⁺CD44^{low}CD25^{neg}) were stimulated by plate-bound anti-CD3 (2 µg/ml, 145-

817 2C11, BD Pharmingen) and anti-CD28 (2 µg/ml, 37.51, BD Pharmingen) in the presence of IL-
818 6 (40 ng/ml) and rhTGF-β1 (2 ng/ml). To determine the influence of indole-3 lactic acid on
819 T_H17 cell differentiation, cells were cultured with vehicle (0.1% Ethanol) or 10-500 µM indole-
820 3-lactic acid (ILA) for 96h under isotonic or hypertonic (+40 mM NaCl) conditions.

821

822 **DNA extraction from feces and qPCR of 16S rRNA genes**

823 DNA from stool samples was isolated using QIAamp DNA Stool Mini Kit (Qiagen) according
824 to the manufacturer's instructions. To optimize bacterial community structure representation, a
825 mutanolysin (Sigma) digestion step was included (6 µl of 25kU/ml stock/sample)⁶⁹. qPCR on a
826 7500 Sequence Detector (Applied Biosystems, AB) was used to enumerate bacterial 16S rRNA
827 gene copies in the genomic DNA extracted from stool samples. Samples were quantified in 10
828 µl reactions containing 1x SYBR Green Master Mix (AB), 300 nM of each primer and 4 ng of
829 genomic DNA. Standard curves for quantification consisted in ten-fold serial dilutions in the
830 range of 10⁸ to 10⁰ copies of *E. coli* (Invitrogen, C404010) or *L. murinus* isolate 16S rRNA
831 gene amplified with primers 27F (5'- GTTTGATCCTGGCTCAG-3') and 1492R (5'-
832 CGGCTA CCTTGTTACGAC-3')⁷⁰. The total amount of bacterial 16S in stool samples was
833 quantified with the universal primers Univ 337F 5'-ACTCCTACGGGAGGCAGCAGT-3' and
834 Univ 518R 5'-GTATTACCGCGGCTGCTGGCAC-3'⁷¹. The total amount of different
835 *Lactobacillus* DNA in stool samples was quantified using the following primers: *L.*
836 *murinus/animalis*⁷² LactoM-F (5'-TCGAACGAACTTCTTTATCACC-3'), LactoM-R (5'-
837 CGTTCGCCACTCAACTCTTT-3'); *L. brevis*⁷³ LbrevF (5'-
838 TGCACTGATTTCAACAATGAAG-3'), LbrevR (5'-CCAGAAGTGATAGCCGAAGC-3');
839 *L. casei/paracasei*⁷⁴ LcaseF (5'-GCACCGAGATTCAACATGG-3'), LcaseR (5'-
840 GGTTCCTGGATCTATGCGGTATTAG-3'); *L. delbrueckii*⁷⁴ LdelbF (5'-
841 GGGTGATTTGTTGGACGCTAG-3'), LdelbR (5'-GCCGCCTTTCAAACCTTGAATC-3'); *L.*
842 *fermentum*⁷⁵ LfermF (5'-GCACCTGATTGATTTTGGTTCG-3'), LactoR (5'-

843 GTCCATTGTGGAAGATTCCC-3'); *L. plantarum*⁷⁶ sg-Lpla-F (5'-
844 CTCTGGTATTGATTGGTGCTTGCAT-3'), sg-Lpla-R (5'-
845 GTTCGCCACTCACTCAAATGTA AAA-3'); *L. rhamnosus*⁷⁴ LrhamF (5'-
846 TGCTTGCATCTTGATTTAATTTTG-3'), LactoR (5'-GTCCATTGTGGAAGATTCCC-3');
847 *L. salivarius*⁷⁵ LsalivF (5'-CGAAACTTTCTTACACCGAATGC-3'), LactoR (5'-
848 GTCCATTGTGGAAGATTCCC-3'). All measurements were performed in duplicates.

849

850 **Code availability.** Code used for the 16S rDNA data analysis has been uploaded to a github
851 repository (<https://github.com/almlab/analysis-salt-responsive>). Software was obtained from
852 publicly available sources; papers describing the software are cited in the text.

853

854 **Data availability.** Raw files of the bacterial V4-V5 16S rRNA data and the *L. murinus* genome
855 have been uploaded to the NCBI Sequence Read Archive as Bioproject PRJNA400793. Raw
856 metagenomic data of the human study are available in the European Nucleotide Archive (ENA,
857 accession number PRJEB22348). Reference datasets for the human metagenome analysis are
858 accessible via ENA (accession number ERP009422) and via <http://hmpdacc.org/>. Numerical
859 source data for all figures are provided with the paper.

860

861 **Statistics**

862 Power calculation is a prerequisite for any animal experiment according to the local animal law
863 and was performed using G*Power Software Version 3.1.9.2. Effect sizes were calculated from
864 previously published experiments. Animals were randomly assigned to the respective body
865 weight-matched groups, probiotic and control treatment were administered without knowledge
866 of the treatment groups. The human pilot study was performed in an unblinded manner. Data
867 analysis was performed by the investigators without knowledge of the treatment groups or
868 treatment phase, respectively. All findings shown have been reproduced in at least two

869 independent experiments. Data are presented depending on their scale and distribution with
870 arithmetic mean and standard deviation (mean \pm s.e.m.) or median including 25-75% quartiles
871 (25|75). Unless otherwise specified, boxplots show median and interquartile range (IQR) with
872 whiskers showing minimum and maximum values, bar graphs show mean \pm s.e.m. Outliers
873 identified by Grubbs' test were excluded. Normality was assessed by Kolmogorov-Smirnov
874 test. To compare independent measurements, we used a *t*-test and Mann-Whitney U test, as
875 appropriate. To compare dependent measurements, we used a paired *t*-test or Wilcoxon signed-
876 rank test, as appropriate. To compare more than two groups, we used one-way ANOVA
877 followed by Tukey's post-hoc test or Kruskal-Wallis test followed by Dunn's post hoc test, as
878 appropriate. Statistical analysis was performed using GraphPad Prism 6. *Lactobacillus* survival
879 times are visualized by Kaplan-Meier curves and statistically compared by Log-rank test.

880 To analyze mouse blood pressure telemetry data, we conducted repeated measurements analysis
881 by using linear mixed models. We tested a random intercept versus a random intercept-slope
882 model and selected the best-fit model. Data analysis was performed with R (Version 3.1.1 R
883 Foundation, Vienna, Austria) using the packages "lme4" and "nlme". A P value <0.05 was
884 considered statistically significant.

885

886 43 Caporaso, J. G. *et al.* Ultra-high-throughput microbial community analysis on the
887 Illumina HiSeq and MiSeq platforms. *The ISME journal* **6**, 1621-1624,
888 doi:10.1038/ismej.2012.8 (2012).

889 44 Preheim, S. P., Perrotta, A. R., Martin-Platero, A. M., Gupta, A. & Alm, E. J.
890 Distribution-based clustering: using ecology to refine the operational taxonomic unit.
891 *Applied and environmental microbiology* **79**, 6593-6603, doi:10.1128/AEM.00342-13
892 (2013).

893 45 Edgar, R. C. & Flyvbjerg, H. Error filtering, pair assembly and error correction for next-
894 generation sequencing reads. *Bioinformatics* **31**, 3476-3482,
895 doi:10.1093/bioinformatics/btv401 (2015).

896 46 Wang, Q., Garrity, G. M., Tiedje, J. M. & Cole, J. R. Naive Bayesian classifier for rapid
897 assignment of rRNA sequences into the new bacterial taxonomy. *Applied and*
898 *environmental microbiology* **73**, 5261-5267, doi:10.1128/AEM.00062-07 (2007).

899 47 Edgar, R. C. Search and clustering orders of magnitude faster than BLAST.
900 *Bioinformatics* **26**, 2460-2461, doi:10.1093/bioinformatics/btq461 (2010).

901 48 Vegan: Community Ecology Package. R package version 2.3-0 (2015).

902 49 Caporaso, J. G. *et al.* PyNAST: a flexible tool for aligning sequences to a template
903 alignment. *Bioinformatics* **26**, 266-267, doi:10.1093/bioinformatics/btp636 (2010).

904 50 Sievers, F. *et al.* Fast, scalable generation of high-quality protein multiple sequence
905 alignments using Clustal Omega. *Molecular systems biology* **7**, 539,
906 doi:10.1038/msb.2011.75 (2011).

907 51 Price, M. N., Dehal, P. S. & Arkin, A. P. FastTree 2--approximately maximum-
908 likelihood trees for large alignments. *PloS one* **5**, e9490,
909 doi:10.1371/journal.pone.0009490 (2010).

910 52 Paradis, E., Claude, J. & Strimmer, K. APE: Analyses of Phylogenetics and Evolution
911 in R language. *Bioinformatics* **20**, 289-290 (2004).

912 53 Freund, Y. & Schapire, R. E. A Decision-Theoretic Generalization of On-Line Learning
913 and an Application to Boosting. *Journal of Computer and System Sciences* **55**, 119-139,
914 doi:10.1006/jcss.1997.1504 (1997).

915 54 Pedregosa, F. *et al.* Scikit-learn: Machine Learning in Python. *Journal of Machine*
916 *Learning Research* **12**, 2825-2830 (2011).

917 55 Breiman, L. Random Forests. *Machine Learning* **45**, 5-32,
918 doi:10.1023/A:1010933404324 (2001).

- 919 56 Pietzke, M., Zasada, C., Mudrich, S. & Kempa, S. Decoding the dynamics of cellular
920 metabolism and the action of 3-bromopyruvate and 2-deoxyglucose using pulsed stable
921 isotope-resolved metabolomics. *Cancer & metabolism* **2**, 9, doi:10.1186/2049-3002-2-
922 9 (2014).
- 923 57 Kuich, P. H., Hoffmann, N. & Kempa, S. Maui-VIA: A User-Friendly Software for
924 Visual Identification, Alignment, Correction, and Quantification of Gas
925 Chromatography-Mass Spectrometry Data. *Frontiers in bioengineering and*
926 *biotechnology* **2**, 84, doi:10.3389/fbioe.2014.00084 (2014).
- 927 58 Hartemink, R., Domenech, V. R. & Rombouts, F. M. LAMVAB—A new selective
928 medium for the isolation of lactobacilli from faeces. *Journal of microbiological methods*
929 **29**, 77-84, doi:10.1016/S0167-7012(97)00025-0 (1997).
- 930 59 Gomila, M. *et al.* Genotypic and phenotypic applications for the differentiation and
931 species-level identification of achromobacter for clinical diagnoses. *PloS one* **9**,
932 e114356, doi:10.1371/journal.pone.0114356 (2014).
- 933 60 Itani, H. A. *et al.* CD70 Exacerbates Blood Pressure Elevation and Renal Damage in
934 Response to Repeated Hypertensive Stimuli. *Circulation research* **118**, 1233-1243,
935 doi:10.1161/CIRCRESAHA.115.308111 (2016).
- 936 61 Atarashi, K. & Honda, K. Analysis of murine lamina propria TH17 cells. (2008).
- 937 62 Wiig, H. *et al.* Immune cells control skin lymphatic electrolyte homeostasis and blood
938 pressure. *The Journal of clinical investigation* **123**, 2803-2815, doi:10.1172/JCI60113
939 (2013).
- 940 63 Mahler, A. *et al.* Increased catabolic state in spinocerebellar ataxia type 1 patients.
941 *Cerebellum* **13**, 440-446, doi:10.1007/s12311-014-0555-6 (2014).
- 942 64 Sunagawa, S. *et al.* Metagenomic species profiling using universal phylogenetic marker
943 genes. *Nature methods* **10**, 1196-1199, doi:10.1038/nmeth.2693 (2013).

944 65 Kultima, J. R. *et al.* MOCAT2: a metagenomic assembly, annotation and profiling
945 framework. *Bioinformatics*, doi:10.1093/bioinformatics/btw183 (2016).

946 66 Segata, N. *et al.* Metagenomic microbial community profiling using unique clade-
947 specific marker genes. *Nature methods* **9**, 811-814, doi:10.1038/nmeth.2066 (2012).

948 67 Therneau, T. M. *A Package for Survival Analysis in S. Version 2.38.* (2015).

949 68 Therneau, T. M. & Grambsch, P. M. *Modeling Survival Data: Extending the Cox Model.*
950 (Springer-Verlag New York, 2000).

951 69 Yuan, S., Cohen, D. B., Ravel, J., Abdo, Z. & Forney, L. J. Evaluation of methods for
952 the extraction and purification of DNA from the human microbiome. *PloS one* **7**,
953 e33865, doi:10.1371/journal.pone.0033865 (2012).

954 70 Caesar, R., Tremaroli, V., Kovatcheva-Datchary, P., Cani, P. D. & Backhed, F.
955 Crosstalk between Gut Microbiota and Dietary Lipids Aggravates WAT Inflammation
956 through TLR Signaling. *Cell metabolism* **22**, 658-668, doi:10.1016/j.cmet.2015.07.026
957 (2015).

958 71 Bergstrom, A. *et al.* Introducing GUT low-density array (GULDA): a validated approach
959 for qPCR-based intestinal microbial community analysis. *FEMS microbiology letters*
960 **337**, 38-47, doi:10.1111/1574-6968.12004 (2012).

961 72 Bindels, L. B. *et al.* Restoring specific lactobacilli levels decreases inflammation and
962 muscle atrophy markers in an acute leukemia mouse model. *PloS one* **7**, e37971,
963 doi:10.1371/journal.pone.0037971 (2012).

964 73 Duniere, L. *et al.* Impact of adding *Saccharomyces* strains on fermentation, aerobic
965 stability, nutritive value, and select lactobacilli populations in corn silage. *Journal of*
966 *animal science* **93**, 2322-2335, doi:10.2527/jas.2014-8287 (2015).

967 74 Byun, R. *et al.* Quantitative analysis of diverse *Lactobacillus* species present in
968 advanced dental caries. *Journal of clinical microbiology* **42**, 3128-3136,
969 doi:10.1128/JCM.42.7.3128-3136.2004 (2004).

970 75 Cui, Y. *et al.* Different Effects of Three Selected *Lactobacillus* Strains in Dextran
971 Sulfate Sodium-Induced Colitis in BALB/c Mice. *PloS one* **11**, e0148241,
972 doi:10.1371/journal.pone.0148241 (2016).

973 76 Matsuda, K. *et al.* Establishment of an analytical system for the human fecal microbiota,
974 based on reverse transcription-quantitative PCR targeting of multicopy rRNA
975 molecules. *Applied and environmental microbiology* **75**, 1961-1969,
976 doi:10.1128/AEM.01843-08 (2009).

977

978

979

980

981

982 **Extended Data Figure Legends**

983

984 **Extended Data Figure 1. Body weight, food, fluid and sodium chloride (NaCl) intake, and**
985 **intestinal transit in mice fed a NSD or HSD.** Body weight (a), food intake (b), fluid intake
986 (c), NaCl intake from the chow (d), NaCl intake from the drinking water (e) and total NaCl
987 intake (f; sum of NaCl intake from chow and drinking water) in mice fed normal salt diet (NSD,
988 n=8) or high salt diet (HSD, n=8). (g) Measurement of intestinal transit. FVB/N mice were fed
989 NSD (n=8) or HSD (n=9) for 14 days and administered activated charcoal (0.5 g/10 ml in 0.5%
990 methylcellulose; 0.1 ml/10 g body weight by oral gavage). Twenty minutes later mice were
991 euthanized and the distance travelled by charcoal was measured. Bars show mean±s.e.m.,
992 circles represent individual mice. **p<0.01, ****p<0.001 using paired two-tailed Student's *t*
993 test for (a-c), one-tailed Wilcoxon matched-pairs signed rank test for (d-f) and unpaired two-
994 tailed Student's *t* test for (g).

995

996 **Extended Data Figure 2. Fecal microbiome profiles of mice kept on NSD or HSD over**
997 **time.** Taxonomic bar charts showing relative abundance of RDP-based OTUs on indicated
998 days. (a) Mice remaining on NSD for 14 days served as NSD controls. Baseline NSD day -1
999 and NSD day 14 are shown. (b) Separate mice were switched from NSD (days -2 and -1) to
1000 HSD for 14 days, and finally re-exposed to NSD for another 14 days (recovery). For time course
1001 analyses, fecal samples from baseline NSD days (-1 and -2), early (days 1-3) and late (day 14)
1002 HSD days and NSD recovery days (days 15-17, 19, 22, 28) are shown. n=8 mice per group.

1003

1004 **Extended Data Figure 3. HSD alters the fecal microbiome and the fecal metabolite profile.**
1005 (a) Mouse 16S rDNA fecal microbiome samples do not separate by diet in a MDS ordination
1006 (white, NSD samples; black, HSD samples; grey, recovery on NSD). (b) Real-time PCR on
1007 DNA extracted from fecal samples of mice fed NSD or HSD using universal 16S rDNA primers

1008 ($n=8$ fecal samples per group from independent mice, indicated by circles; two-tailed Wilcoxon
1009 matched-pairs signed rank test). **(c)** Phylogenetic tree showing changes in microbiome
1010 composition caused by HSD. OTUs present in samples from day 14 are indicated by colored
1011 circles (red indicates reduction in HSD samples; blue indicates enrichment). The circles' radii
1012 indicate median log fold difference in relative abundance between the two diets. Filled circles
1013 mark statistically significant differences (two-tailed Student's t -test, Benjamini-Hochberg
1014 correction, $p<0.05$). **(d-g)** High dietary salt strongly influences the fecal metabolite profile.
1015 Male FVB/N mice ($n=8$) were fed a NSD and then switched to HSD. Metabolites were extracted
1016 from fecal pellets taken under NSD (day -3) and HSD (day 13), and analyzed by gas-
1017 chromatography mass-spectrometry. **(d)** HSD samples are clearly distinguishable from NSD
1018 samples in a principal component analysis for fecal metabolites. **(e)** Fecal metabolites clearly
1019 cluster by treatment. The majority of fecal metabolites are reduced by HSD. Hierarchically
1020 clustered heatmap, metabolites shown in alphabetical order. Metabolites were normalized by
1021 subtracting the minimum and dividing by the maximum value across all mice. **(f)** Fecal levels
1022 of the nucleoside adenosine were similar in both diets, suggesting that the change in metabolites
1023 is not due to a decrease in overall bacterial biomass. **(g)** HSD leads to a reduction in total
1024 metabolite peak intensities in fecal samples. **** $p<0.01$ two-tailed paired Student's t -test for (f,**
1025 **g).**

1026

1027 **Extended Data Figure 4. Accuracy of AdaBoost and Random Forest classifiers. (a)**
1028 AdaBoost and random forest classifiers (trained on samples from days -2, -1, and 14) were used
1029 to predict the classification of all samples from HSD mice. The fraction of samples from each
1030 time point that the classifiers predicted as belonging to animals currently on a HSD is shown.
1031 The two runs of the random forest produced the same fractions, so only one line is shown for
1032 the two random forest classifiers. **(b)** Time series for the other remaining 7 OTUs important to
1033 the classifier. NSD and HSD phases are indicated by white and grey backgrounds. Mice ($n=12$)

1034 were switched from NSD to HSD and back to NSD (subgroup of $n=8$). Other control mice ($n=8$)
1035 remaining on NSD shown in white. Boxplots: median, IQR, whiskers $1.5 \times \text{IQR}$, circles represent
1036 samples from independent mice.

1037

1038 **Extended Data Figure 5. *L. murinus* genome and *in vitro* growth of *Lactobacilli*.** (a) Venn
1039 diagram of the coding sequences present in the *L. murinus* and two other isolates with available
1040 with full genome sequences. (b) Bootstrapped phylogenetic tree of full-length 16S rDNA from
1041 a variety of *Lactobacillus* species resident to rodent or human guts. Prevalence of the respective
1042 species in the MetaHIT cohort is shown. *L. murinus* strains are absent in the MetaHIT cohort.
1043 (c) Growth yield (OD_{600}) of *L. murinus* measured at increasing concentrations of NaCl. Aerobic
1044 endpoint measurements of liquid *L. murinus* cultures in MRS medium and increasing NaCl
1045 concentrations relative to growth in MRS without the addition of NaCl. $n=5$ independent
1046 experiments. (d) Anaerobic growth yield of *L. murinus*, *A. muciniphila*, *P. excrementihominis*,
1047 and *C. difficile* grown at 37 °C for 48 hours in MGAM liquid medium. Growth at each salt
1048 concentration is normalized to growth at 0.086 M Na^+ . The respective IC_{50} is indicated. $n=3$
1049 technical replicates across 2 experiments. (e) Anaerobic growth of selected
1050 human *Lactobacilli* in MGAM medium with increasing NaCl concentrations. Relative growth
1051 yield is calculated based on AUCs by comparing to growth in MGAM without the addition of
1052 NaCl. $n=3$ independent experiments with 3 technical replicates. (f) Heatmap showing data as
1053 in (e). The respective IC_{50} is shown in the bottom row. (g) Growth yield of *E. coli* and *L.*
1054 *murinus*, grown at 37 °C for 12-16 hours on LB (*E.coli*) or MRS broth (*L. murinus*). $n=4$
1055 technical replicates from two independent experiments. Mean \pm s.e.m.

1056

1057 **Extended Data Figure 6. Indole metabolites in murine fecal samples.** (a) Effect of HSD on
1058 fecal indole-3 acetic acid (IAA) and (b) indole-3 carboxaldehyde (IAld) content in FVB/N mice
1059 fed a NSD or HSD ($n=12$ per group in **b**; $n=13$ per group in **c**). (c-d) Germ-free (GF) mice

1060 monocolonized with *L. murinus* showed increased fecal IAA and IAld content ($n=8$ per group).
1061 * $p<0.05$ using one-tailed Wilcoxon matched-pairs signed rank test for **(a-b)**, **** $p<0.0001$
1062 using one-tailed Mann-Whitney U test for **(c)** and **** $p<0.0001$ using unpaired one-tailed
1063 Student's t-test for **(d)**. n represents independent mice.

1064

1065 **Extended Data Figure 7. The effect of *Lactobacilli* on actively-induced EAE.** **(a)** Median
1066 cumulative clinical EAE scores at day 15, 16 and 17 post immunization (p.i.) of NSD ($n=9$),
1067 HSD ($n=11$) and HSD mice treated with *L. murinus* ($n=6$) starting at the day of immunization.
1068 Kruskal-Wallis followed by Dunn's multiple comparisons test * $p<0.05$, ** $p<0.01$, *** $p<0.001$.
1069 n represents independent mice, indicated by circles. **(b)** Clinical course of MOG₃₅₋₅₅ EAE in
1070 NSD mice (black circles, $n=7$) and NSD mice treated with *L. murinus* (green squares, $n=4$.
1071 Mean \pm s.e.m.). * $p<0.05$ using two-tailed Mann-Whitney U test. **(c)** Clinical course of MOG₃₅₋
1072 ₅₅ EAE in HSD mice (black circles) and HSD mice treated with *L. reuteri* (green squares, $n=6$
1073 independent mice per group, mean \pm s.e.m.). * $p<0.05$ using two-tailed Mann-Whitney U test.
1074 **(d-e)** Quantification for CD4⁺IL-17A⁺IFN- γ cells on day 17 of EAE in the spleen **(d)** and spinal
1075 cord **(e)**. $n=4$ independent mice per group. Mean \pm s.e.m. * $p<0.05$ one-tailed Mann-Whitney U
1076 test. **(f-h)** Spinal cords on day 17 of EAE were analyzed by real-time RT-PCR for relative
1077 expression of *Il17a* **(f)**, $n=7$ for NSD, $n=6$ for HSD and $n=5$ for HSD+*L. murinus*), *Rorc* **(g)**, $n=5$
1078 for NSD, $n=6$ for HSD and $n=5$ for HSD+*L. murinus*) and *Csf2* **(h)**, $n=8$ for NSD, $n=6$ for HSD
1079 and $n=4$ for HSD+*L. murinus*). Mean \pm s.e.m. * $p<0.05$, ** $p<0.01$ using one-way ANOVA
1080 followed by Tukey's post-hoc test. **(i)** Quantification of IFN- γ -producing T_H1 cells in siLPL on
1081 day 3 of EAE ($n=4$ per group) and quantification of IFN- γ producing T_H1 cells in spleen ($n=4$
1082 per group) and spinal cord on day 17 of EAE ($n=5$ for NSD, $n=6$ for HSD and $n=5$ for HSD+*L.*
1083 *murinus*). n indicates number of independent mice per group. Mean \pm s.e.m. ns=not significant
1084 by one-way ANOVA. **(j-m)** Fecal indole metabolites were determined in MOG₃₅₋₅₅ EAE mice
1085 by LC-MS/MS analysis. Effect of HSD on fecal IAA **(j)** and IAld **(k)** content on day 10 p.i.

1086 ($n=5$ per group for **j**, $n=4$ for NSD and $n=5$ for HSD in **k**). Fecal IAA (**l**) and IAld (**m**) content
1087 in MOG₃₅₋₅₅ EAE mice fed HSD with or without concomitant *L. murinus* treatment on day 10
1088 p.i. ($n=7$ per group for **l**, $n=8$ for HSD and $n=7$ for HSD+*L. murinus* for **m**). * $p<0.05$ using
1089 unpaired one-tailed Student's *t*-test for (**j and l-m**) and one-tailed Wilcoxon matched-pairs
1090 signed rank test for (**k**). *n* indicates number of independent mice per group.

1091

1092 **Extended Data Figure 8. Actively-induced EAE in gnotobiotic mice.** (**a, b**) HSD fails to
1093 induce intestinal T_H17 cells in germ-free MOG₃₅₋₅₅ EAE mice ($n=5$ for GF+NSD and $n=6$ for
1094 GF+HSD). (**a**) Analysis of IL-17A and IFN- γ in CD4⁺ siLPL isolated from NSD or HSD-fed
1095 MOG₃₅₋₅₅ immunized germ-free mice (day 3 p.i.). Representative flow cytometry plots (left)
1096 show one mouse per group. Quantifications show frequencies of CD4⁺IL-17A⁺IFN- γ ⁻ (middle)
1097 and CD4⁺IL-17A⁺IFN- γ ⁺ (right) cells and (**b**) CD4⁺ ROR γ t⁺ frequencies in siLPL. (**c-d**) *L.*
1098 *murinus* reduces small intestinal (siLPL) and colonic (cLPL) lamina propria T_H17 cells in EAE
1099 mice colonized with segmented filamentous bacteria (SFB). MOG₃₅₋₅₅ EAE was induced in GF
1100 mice monocolonized with SFB (GF+SFB) and GF mice colonized with SFB and *L. murinus*
1101 (GF+SFB+*L. murinus*). LPL were isolated on day 3 p.i. (**c**) Left panel shows representative
1102 flow cytometry plots demonstrating IL-17A and IFN- γ expression in CD4⁺ siLPL (one mouse
1103 per group). Middle panel shows quantification of CD4⁺IL-17A⁺IFN- γ ⁻ siLPL ($n=9$ for
1104 GF+SFB, $n=8$ for GF+SFB+*L. murinus*). Right panel shows quantification of CD4⁺ROR γ t⁺
1105 siLPL ($n=9$ mice per group). (**d**) Left panel shows representative flow cytometry plots (one
1106 mouse per group) depicting IL-17A and IFN- γ expression in CD4⁺ cLPL. Middle and right
1107 panel show quantification of CD4⁺IL-17A⁺IFN- γ ⁻ ($n=8$ for GF+SFB, $n=9$ for GF+SFB+*L.*
1108 *murinus*) and CD4⁺ IL-17A⁺IFN- γ ⁺ cLPL ($n=8$ per group). All bar graphs show mean \pm s.e.m,
1109 circles represent independent mice. * $p<0.05$, *** $p<0.001$ unpaired one-tailed Student's *t*-test
1110 for (**a-d**).

1111

1112 **Extended Data Figure 9. Treatment with *L. murinus* or *L. reuteri* ameliorates salt-sensitive**
1113 **hypertension. (a)** Mean diastolic pressures over time in response to HSD and HSD with
1114 concomitant *L. murinus* treatment in $n=7$ FVB/N mice. Scale bar indicates 24 hours. Horizontal
1115 line indicates the mean across all values of the respective phase. **(b, c)** Mean systolic **(b)** and
1116 diastolic **(c)** blood pressures in these mice ($n=7$) fed a HSD (black curve) and HSD with
1117 concomitant *L. murinus* treatment at circadian scale. Arrows indicate the time of *L. murinus*
1118 gavage. **(d, e)** Boxplots (median, IQR, whiskers $1.5 \times \text{IQR}$) show systolic **(d)** and diastolic **(e)**
1119 blood pressures recorded continuously in FVB/N mice fed a HSD and a HSD with concomitant
1120 *L. reuteri* treatment. These mice ($n=9$) were fed a HSD for 10 days prior to concomitant *L.*
1121 *reuteri* treatment for another 7 days. $***p < 0.001$ vs. HSD using linear mixed model. **(f, g)**
1122 Boxplots (median, IQR, whiskers $1.5 \times \text{IQR}$) show systolic **(f)** and diastolic **(g)** blood pressures
1123 in mice ($n=5$) fed a HSD and a HSD with concomitant *Escherichia coli* Nissle 1917 (*E. coli*)
1124 treatment for 3 days, respectively. Statistics using linear mixed model. **(h-j)** Quantification of
1125 $\text{CD4}^+ \text{IL-17A}^- \text{IFN-}\gamma^+$ lymphocytes in siLPL **(h)**, $n=5$ for NSD, $n=7$ for HSD, $n=6$ for HSD+*L.*
1126 *murinus*) and cLPL and spleen, respectively **(i-j)**, $n=5$ for NSD, $n=6$ for HSD, $n=6$ for HSD+*L.*
1127 *murinus*). All bars show mean \pm s.e.m, circles represent independent mice. $*p < 0.05$ using
1128 Kruskal-Wallis and Dunn's post-hoc test for **(h)**, one-way ANOVA for **(i-j)**.

1129

1130 **Extended Data Figure 10. High salt challenge in healthy human subjects. (a)** Total salt
1131 intake according to dietary records ($n=12$, paired one-tailed t -test). **(b, c)** Metagenome analysis
1132 shows loss of *Lactobacillus* gut populations during human high salt challenge. Shown are all
1133 subjects (horizontal axis) for which gut *Lactobacilli* were detected at baseline and all species
1134 so detected (vertical axis) using the mOTU **(b)** or MetaPhlAn framework **(c)** for bacterial
1135 species identification. Heatmap cells show abundance for mOTU (insert counts as fraction of
1136 sample total) or average coverage (reads per position) for MetaPhlAn of these *Lactobacilli* at
1137 baseline (left part of cells, black border) and after high salt challenge (right part of cells, grey

1138 border). Cross markers show complete loss (nondetection after high salt challenge) of each
1139 species. In all cases but one (shown), baseline *Lactobacillus* populations are no longer detected
1140 post high salt. **(d)** qPCR using *Lactobacillus*-specific 16S rDNA primers in human fecal
1141 samples positive for *Lactobacillus* at baseline show a loss of the respective species after 14 days
1142 of high salt. *Lactobacillus* 16S rDNA copy number in 4 ng fecal DNA is shown. Symbols
1143 indicate study subject, colors indicate respective *Lactobacillus* species. **(e)** Kaplan-Meier
1144 survival curves contrasting the fate of gut *Lactobacillus* populations (detected using the mOTU
1145 framework) following high salt challenge (bright red curve) and in healthy control individuals
1146 from reference cohorts ($n=121$, see methods) not undergoing any intervention (bright blue
1147 curve). This is compared with corresponding survival curves over time for the set of all other
1148 detected gut bacterial species following high salt challenge (high salt-others, dark red curve)
1149 and without such challenge in controls (NSD-others, dark blue curve). **(f)** For a clearer view of
1150 its time range only the salt intervention curves from **(e)** are shown. Two observations are clear.
1151 First, *Lactobacillus* on average persist for shorter times in the gut than the average over all other
1152 species. Second, a high salt challenge strongly increases gut loss of both *Lactobacillus* and non-
1153 *Lactobacillus* species. As such, in combination, *Lactobacillus* loss is highly pronounced under
1154 high salt intervention and significantly ($p<1.62e-8$) faster than the average over all species. **(g-**
1155 **i)** Metagenome analysis shows introduction of novel *Lactobacillus* gut populations during
1156 human high salt challenge. Shown are all subjects (horizontal axis) for which gut *Lactobacilli*
1157 were detected following high salt challenge, and all species so detected (vertical axis) using the
1158 SpecI **(g)**, mOTU **(h)** or MetaPhlAn **(i)**. Heatmap cells show abundance (insert counts as
1159 fraction of sample total for SpecI and mOTU) and average coverage (reads per position for
1160 MetaPhlAn) of these *Lactobacilli* at baseline (left part of cells, black border) and after high salt
1161 challenge (right part of cells, gray border). Cross markers show novel introduction
1162 (nondetection at baseline) of each species.

1163

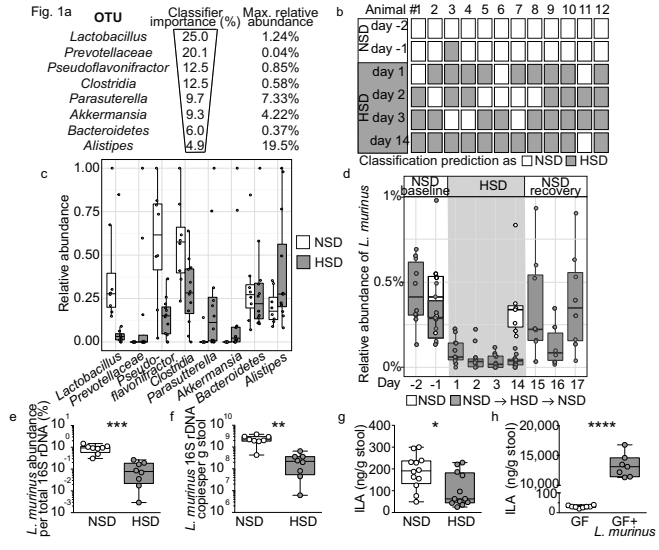


Fig. 2a

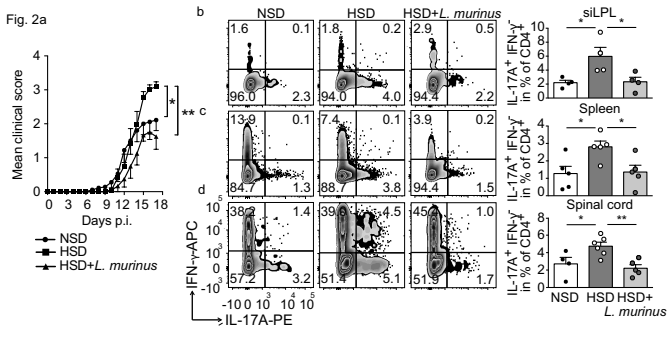
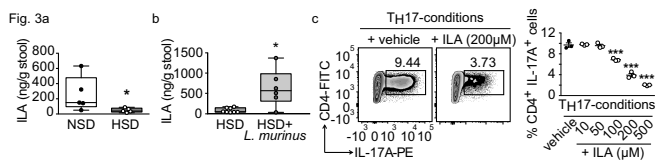


Fig. 3a



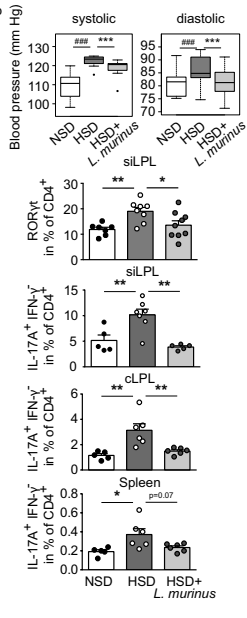
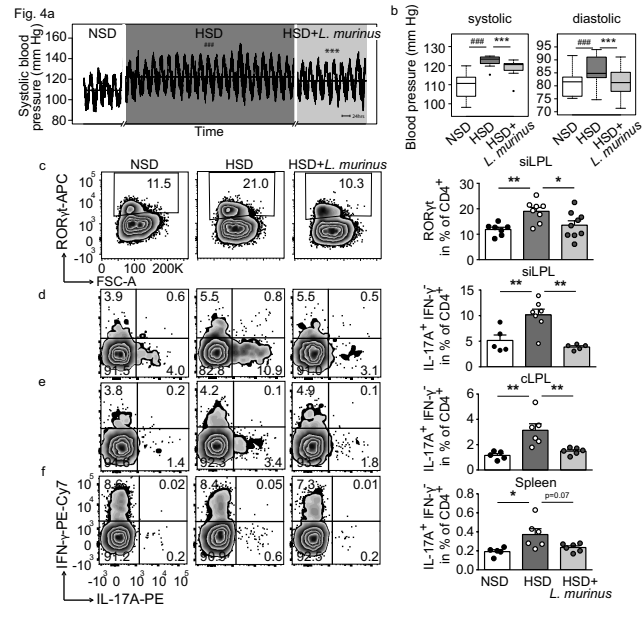
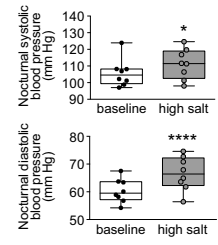
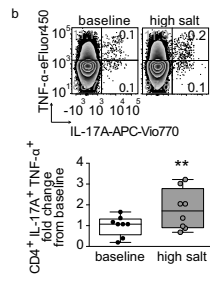


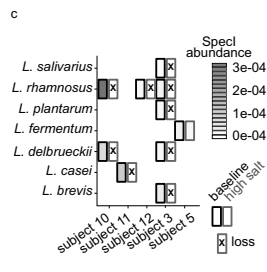
Fig. 5a



b



c



d

